The interaction of p130Cas with PKN3 promotes malignant growth

Authors: Jakub Gemperle[1], Michal Dibus[1], Lenka Koudelková[1], Keziban Unsal-Kacmaz[2], Daniel Rosel[1], Jan Brábek[1]*

1 Department of Cell Biology, Faculty of Science, Charles University in Prague, Czech Republic
2 Oncology Research Unit, Bristol-Myers Squibb, University of North Carolina at Chapel Hill, Princeton, New Jersey

* correspondence should be directed to Jan Brábek (jan.brabek@natur.cuni.cz)

Abstract

Protein p130Cas is an adaptor protein mainly implied in integrin signaling downstream of Src kinase. Due to its modular structure p130Cas acts as a general regulator of cancer cell growth and invasiveness induced by different oncogenes. Besides involvement in integrin-mediated signaling, however, p130Cas signaling leading to malignant progression is not well known.
In this study, we show a novel interaction of p130Cas with Ser/Thr kinase PKN3 which is implicated in tumor growth of prostate and breast cancer cells downstream of phosphoinositide 3-kinase. This interaction is direct and is mediated by p130Cas SH3 domain and centrally located polyproline sequence of PKN3. PKN3 is the first Ser/Thr kinase identified not only to bind p130Cas, but also showed to be able to phosphorylate p130Cas in vitro. We demonstrate that PKN3 colocalizes with p130Cas in pro-invasive structures, lamellipodia and podosome rosettes, and that PKN3-p130Cas interaction increases PKN3-driven invasiveness and growth of mouse embryonic fibroblasts (MEFs) and MEFs transformed by Src oncogene. Furthermore, we show the importance of PKN3-p130Cas interaction for tumor growth of Src-transformed cells in vivo. Taken together, our results suggest that the PKN3-p130Cas complex may represent an attractive therapeutic target in late-stage malignancies.

Keywords: PKN3, p130Cas, BCAR1, CAS, Src, SH3

Introduction

p130Cas (Crk associated substrate, CAS) is a molecular scaffold involved in regulation of several processes, such as cell survival, migration, invasivity and proliferation in both normal and pathological cells (reviewed in ref. Cabodi, del Pilar Camacho-Leal, *et al.*, 2010; Tikhmyanova, Little and Golemis, 2010). Due to its modular structure, p130Cas plays a crucial role in signaling originating from many mutated or amplified oncogenes (Tikhmyanova, Little and Golemis, 2010; Nikonova *et al.*, 2014; Tornillo, Defilippi and Cabodi, 2014). It has been reported that knockdown of p130Cas leads to proliferative arrest in breast cancer cell lines carrying oncogenic mutations in BRAF, KRAS, PTEN or PIK3CA (Pylayeva *et al.*, 2009). Moreover, its involvement in Src-mediated tumorigenesis has been clearly demonstrated. Src-transformed MEFs exhibit increased capability to invade through Matrigel and induce metastases in mice (Honda *et al.*, 1998; Brábek *et al.*, 2004, 2005). Other experiments in vivo have shown that p130Cas also drives growth, aggressiveness and progression of ErbB2 overexpressing breast tumors, including metastatic colonization of lungs (Cabodi *et al.*, 2006; Cabodi, Tinnirello, *et al.*, 2010). Correspondingly, elevated expression of p130Cas in human patients is associated with early disease recurrence and poor prognosis in several cancer types including lung, prostate, pancreas, ovarian and mammary cancers (Defilippi, Di Stefano and Cabodi, 2006; Fromont *et al.*, 2007; Cabodi, del Pilar Camacho-Leal, *et al.*, 2010; Tikhmyanova, Little and Golemis, 2010; Fromont and Cussenot, 2011; Nick *et al.*, 2011; Nikonova *et al.*, 2014) and is linked with hormone deprivation-resistance to the anti-tumor drugs (standard therapeutics) such as adriamycin (doxorubicin) and tamoxifen (Dorssers *et al.*, 2001; Ta *et al.*, 2008). Taken together, these evidences clearly underline a role for p130Cas as a general regulator of cancer cell growth and metastasis induced by different oncogenes.

The structure of p130Cas consists of N-terminal SRC homology 3 (SH3) domain, substrate domain (SD) and serine-rich domain (SRD) followed by Src and PI3K binding region and terminated by CAS-family C-terminal homology domain (CCH) (reviewed in Cabodi, del Pilar Camacho-Leal, *et al.*, 2010). The majority of known p130Cas downstream signalling is attributed to tyrosine phosphorylation of repeated YXXP motif within p130Cas SD domain (reviewed in Cabodi et al., 2010a and Defilippi et al., 2006). The level of p130Cas tyrosine phosphorylation is mainly dependent on binding capacity of its SH3 domain which facilitates direct interaction of p130Cas with polyproline motif of various phosphatases (PTP1B, PTP-PEST) and kinases (FAK, PYK2) or mediates indirect association with Src via FAK (PYK2) bridge (Astier *et al.*, 1997; Ruest *et al.*, 2001; Fonseca *et al.*, 2004). Specifically, association of p130Cas via p130Cas SH3 domain with FAK and Src at focal adhesions transmits signals that induce lamellipodia and cell migration, support cell proliferation, cell invasiveness and block anoikis (Ruest *et al.*, 2001; Brábek *et al.*, 2005; Defilippi, Di Stefano and Cabodi, 2006; Tazaki *et al.*, 2008; Donato *et al.*, 2010; Nikonova *et al.*, 2014). p130Cas has also been shown to be phosphorylated at serine residues which correlates with invasive cell phenotype and is partially dependent on p130Cas SH3 domain, however, responsible serine/threonine kinases have not been identified yet (Makkinje *et al.*, 2009). In addition, p130Cas has been shown to interact with 14-3-3 proteins in a phosphoserine-dependent manner which takes place mainly at lamellipodia during integrin-mediated cell attachment to the extracellular matrix (ECM) (Garcia-Guzman *et al.*, 1999).

In screen for p130Cas SH3 domain new interaction partners, we have recently predicted a list of candidates and verified p130Cas SH3 binding to polyproline motifs of GLIS2 and DOK7 (Gemperle *et al.*, 2017). From other candidates on the list, we have now selected serine/threonine PKN3 kinase with the polyproline motif P_{500}**P**P**KP**P**R**L for further analysis in detail.

PKN3 is a member of the PKN family, which is part of the protein kinase C (PKC) superfamily of serine/threonine kinases. The role of PKN3 in tumorigenesis was identified in early reports which showed that PKN3 mRNA is scarce in normal human adult tissues, but abundantly expressed in numerous cancer cell lines (Oishi *et al.*, 1999). In contrast, the other members of PKN family PKN1 and PKN2, exhibit ubiquitous expression in human and rat tissues (Mukai and Ono, 1994; Quilliam *et al.*, 1996; Hashimoto *et al.*, 1998). PKN3, but not PKN1 or PKN2, has been shown to regulate malignant prostate cell growth downstream of activated phosphoinositide 3-kinase (PI3K) independent of Akt (Leenders *et al.*, 2004) and, moreover, only PKN3 possess the polyproline sequence in its central part that we have predicted as a potential p130Cas SH3 domain binding site

(Gemperle *et al.*, 2017). In addition, when stimulated in a fatty-acid dependent manner, the catalytic activity of PKN3 was less responsive in comparison to PKN1 and PKN2, thereby highlighting the differences in function of PKN isoforms, as well as their regulation (Oishi *et al.*, 1999).

Using an orthotopic mouse tumor models, the effect of PKN3 on cancer growth was shown by conditional reduction of PKN3 expression in tumors. In all cases downregulation of PKN3 protein impaired primary prostate and breast tumor growth and blocked metastasis (Leenders *et al.*, 2004; Unsal-Kacmaz *et al.*, 2011). Correspondingly, overexpression of exogenous PKN3 in breast cancer cells further increased their malignant behavior in-vitro (Unsal-Kacmaz *et al.*, 2011). Experiments with PKN3 KO generated mice which looks indistinguishable from those of their wild type (WT) counterparts showed also the role of host stromal PKN3 in tumor progression (Mukai *et al.*, 2016). Stromal PKN3 is enriched in primary endothelial cells (also in osteoclasts (Uehara *et al.*, 2017)) which are apart from tumor cells among few normal cell types with significant amount of PKN3, which is consistent with their usually invasive features (Aleku *et al.*, 2008). Systemic administration of siRNA-lipoplex (Atu027) directed against PKN3 that targets mainly stromal compartment rather than pathologically defined tumor entity prevented lung metastasis in lung experimental and spontaneous breast metastasis models in dose-dependent manner (Santel *et al.*, 2010).

In mammalian tissues, the PKN family constitutes some of the main Rho GTPase-associated protein kinase activities (Vincent and Settleman, 1997; Mellor *et al.*, 1998; Lim *et al.*, 2008). Specifically, Unsal-Kacmaz et al. demonstrated that PKN3 physically interacts with Rho-family GTPases, and preferentially with RhoC, a known mediator of tumor invasion and metastasis in epithelial cancers (Unsal-Kacmaz *et al.*, 2011). Besides interaction with RhoC, however, the molecular mechanisms, by which PKN3 contributes to malignant growth and tumorigenesis, are not well understood.

In this study, we have shown that PKN3 directly interacts with p130Cas and phosphorylates it in vitro and potentially in vivo. Furthermore, we have demonstrated the importance of PKN3 – p130Cas interaction for PKN3-stimulated cell growth and invasiveness in vitro and tumor growth in vivo.

Results

p130Cas directly interacts with PKN3

To confirm the predicted PKN3-p130Cas interaction we first analyzed the potential of p130Cas SH3 domains variants to pull-down PKN3 (scheme of p130Cas and PKN3 mutagenesis in Fig. 1A). As predicted, only the p130Cas SH3 WT, but not phosphomimicking mutant variant (Y12E), showed strong association with PKN3 WT. Correspondingly p130Cas SH3 WT was not able to effectively pull-down a PKN3 variant where the target polyproline motif was mutated to P_{500}APSAPRL (PKN3 mPR; Fig. 1B, 10-50x decrease compared to WT; p=0.003). Notably, kinase-inactivating mutation in catalytic domain of mouse PKN3 (KD; K577E, scheme of mutants Fig. 1A, see supplementary figure S1A for the confirmation of kinase inactivity) also caused significant decrease (4-20x; p=0.007) of PKN3 – p130Cas SH3 interaction (Fig. 1B). Subsequently, we confirmed p130Cas - PKN3 interaction using co-immunoprecipitation analysis. We have shown that PKN3 co-precipitates with immunoprecipitated GFP-p130Cas WT and non-phosphorylatable mutant (Y12F) (Fig. 1C), but not with phosphomimicking mutant (Y12E), and that p130Cas co-precipitates strongly with immunoprecipitated PKN3 WT, less with PKN3 KD and almost not with PKN3 mPR (Fig. 1D). Finally, using far-Western experiments, we confirmed that p130Cas-PKN3 interaction is direct. (Fig. 1E, F).

PKN3 colocalizes with p130Cas in lamellipodia and podosome rosettes

To further assess the p130Cas-PKN3 interaction we analyzed co-localization of p130Cas and PKN3 in cells. Namely, we analyzed the dynamic localization of p130Cas and PKN3 in p130Cas-/- MEFs co-expressing GFP-p130Cas, variants of mCherry-PKN3 and CFP-LifeAct. We found that both p130Cas and PKN3 are enriched in lamellipodia of MEFs (Fig. 2A; supplementary movies S1-2 with GFP-PKN3 variants and mCherry-LifeAct). Localization of PKN3-mPR mutant to lamellipodia was slightly, but significantly impaired (Fig. 2A-B), suggesting that polyproline sequence of PKN3 is important for its targeting to lamellipodia. Cells expressing GFP-Flag-PKN3 KD exhibited more pronounced filopodia-like protrusions and the presence of lamellipodia was extremely rare compared to other variants of PKN3 preventing quantification of PKN3 membrane localization (supplementary figure S1B and supplementary movies S3 with GFP-PKN3 KD and mCherry-LifeAct).

PKN3 has been recently shown to localize to specific actin-rich structures called podosome rings and belts in osteoclasts (Uehara *et al.*, 2017). Formation of similar structures called podosome rosettes can be induced in MEFs when transformed by activated Src (SrcF) (Tarone *et al.*, 1985). Importantly, p130Cas was shown to be critical for their formation (Brábek *et al.*, 2004). To investigate if PKN3 localizes to podosome rosettes we expressed the Flag-PKN3 variants in SrcF-transformed MEFs p130Cas-/- re-expressing p130Cas (SC cells) and analyzed their localization using a confocal microscopy on fixed cells. Both PKN3 WT and mPR were enriched in podosome rosettes and co-localized there with p130Cas and actin suggesting that p130Cas is not responsible for PKN3 targeting to podosome rosettes (Fig. 2C).

PKN3 activity is important for stress fibers formation

In life cell imaging/microscopy experiments, we noticed temporary co-localization of GFP-PKN3 WT or mPR with stress fibers (mCherry-LifeAct) (supplementary figure S1B-C). Since PKN3 downregulation in HUVEC cells leads to disruption of stress fibers formation (Mopert et al., 2012) and p130Cas expression has been previously shown to affect stress fibers morphology (Honda *et al.*, 1998), we analyzed the importance of PKN3 activity and interaction with p130Cas on stress fibers formation. Therefore, we co-transfected p130Cas-GFP WT and mCherry-Flag fused PKN3 variants (WT, mPR, KD) or mCherry to p130Cas-/- MEFs (Fig. 3A). Cells expressing PKN3 WT or mPR displayed prominent stress fibers suggesting that interaction between p130Cas and PKN3 is not important for stress fibers formation. In contrast, transfection of cells by PKN3 KD greatly reduced stress fibers formation and instead induced cortical localization of F-actin (Fig. 3A).

p130Cas stimulates PKN3 kinase phosphorylation on T849 independently of p130Cas-PKN3 interaction

It was previously published that PKN3 turn motif site phosphorylation (human Thr860 homologous to mouse Thr849) correlates with PKN3 activity and that active PKN3 is predominantly localized in nucleus (Leenders *et al.*, 2004; Unsal-Kacmaz *et al.*, 2011). To determine, whether p130Cas influences PKN3 activation we analyzed activity of endogenous mouse PKN3 by anti-pThr849 antibody in the presence or absence of protein p130Cas. PKN3 phosphorylation on Thr849 was lower in p130Cas-/- MEFs than in p130Cas-/- MEFs re-expressing p130Cas or transfected by GFP-p130Cas (Fig. 3B-C). The expression of Y12E variant of GFP-p130Cas, which doesn't bind PKN3, also increased Thr849 phosphorylation of PKN3. Consistently, PKN3 mPR mutant unable to bind p130Cas didn't differ in pThr849 phosphorylation status from PKN3 WT (Fig. 3D-E). Surprisingly, Thr849 phosphorylation was not increased by expression of GFP-p130Cas without CCH domain (dCCH) (Fig. 3A-B and supplementary figure S2D). PKN3 KD used as negative control of anti-pThr849 antibody specificity was not phosphorylated as expected (Fig. 3D). Taken together, the data suggest that p130Cas expression induces PKN3 activation and this activation is independent of p130Cas – PKN3 interaction.

p130Cas - PKN3 co-expression and p130Cas Ser428(432) and PKN3 Thr860 phosphorylation are positively correlated in human breast (prostate) tumors

Previous studies showed positive correlation between PKN3 or p130Cas/BCAR1 protein levels and the cancer progression in breast and prostate cancer patients (Oishi *et al.*, 1999; Dorssers *et al.*, 2004; Leenders *et al.*, 2004; Fromont and Cussenot, 2011; Strumberg *et al.*, 2012; Nikonova *et al.*, 2014; Schultheis *et al.*, 2014). To test the assumed link between PKN3 and p130Cas signaling we further performed cross-correlation analysis of publicly available transcriptomic data using the cBio Cancer Genomics Portal (cbioportal.org) (Gao *et al.*, 2013). We focused on invasive breast carcinoma (1100 tumors in TCGA, provisional) and prostate adenocarcinoma studies (499 tumors, TCGA, provisional). On these sets of RNA seq data we evaluated expression of PKN3 and p130Cas/BCAR1 and run correlation statistical analysis (Fig. 4D-F). This analysis showed that elevated expression of PKN3 significantly positively correlates with the elevated expression of p130Cas/BCAR1 and vice versa in both breast cancer and prostate cancer patients (Fig. 4A, supplementary figure S2A). Similarly, the level of p130Cas/BCAR1 expression is increasing with the level of Src kinase whose signaling is highly connected with p130Cas/BCAR1 (Brábek *et al.*, 2004; Fonseca *et al.*, 2004); Fig. 4B, Supplementary figure S2B). In contrast, expression of PKN2 that does not possess p130Cas interaction site and therefore do not suggest crosstalk with p130Cas/BCAR1 signaling circuit has negative correlation to p130Cas/BCAR1 mRNA level (Figure 4C; Supplementary figure S2C, summary table in S2D). In parallel we analyzed the available data on protein phosphorylation levels of PKN3 and p130Cas/BCAR1 (Clinical Proteomic Tumor Analysis Consortium (CPTAC), MS analysis of 34 invasive breast carcinoma tumors). Statistical analysis revealed that phosphorylation of PKN3 at Thr860 (reflects PKN3 activity, homologous to mouse Thr849) and p130Cas/BCAR1 at Ser428 (conserved homolog to mouse Ser432, in cBioportal analysis shown for p130Cas/BCAR1 as Ser474) exhibits strong positive correlation (Pearson test 0,42 with p value 0,0134, Spearman test 0,434 with p value 0,0106; Fig. 4D). Taken together, the cross-correlation analysis of the transcriptomic and phosphoproteomic data shows a positive correlation between PKN3 and p130Cas/BCAR1 expression in invasive breast carcinoma and prostate adenocarcinoma tumors, and positive correlation between PKN3 activity and the level of p130Cas/BCAR1 phosphorylation on Ser428 in invasive breast carcinoma tumors.

PKN3 phosphorylates mouse p130Cas on Ser432

In addition to tyrosine phosphorylation, p130Cas has been previously reported to undergo serine phosphorylation under various conditions, e.g. during mitosis or cell adhesion, however the kinase responsible for the phosphorylation has not been identified yet (Garcia-Guzman et al., 1999; Makkinje et al., 2009; Yamakita et al., 1999). Our cross-correlation analysis of the transcriptomic and phosphoproteomic data showed that phosphorylation of human p130Cas/BCAR1 on Ser428 correlates with increased PKN3 activity, indicating that PKN3 could be responsible for this phosphorylation. Human Ser428 of p130Cas/BCAR1 corresponds to mouse p130Cas Ser432 which has conserved

surrounding sequence (KRL**S**A) and fits well to the known PKN3 phosphorylation motif (Collazos et al., 2011). Ser432 is, similarly as the majority of p130Cas potential Ser/Thr phosphorylation sites, localized in p130Cas SRD domain. To test the assumed ability of PKN3 to phosphorylate p130Cas, we have prepared GFP fused p130Cas mutant in Ser432 (S432A) and p130Cas mutated in SRD in a way that all 15 Ser/Thr were substituted with Ala or Asn (15AN). The substitution of several Ser/Thr to Asn, instead of more common substitution to Ala, was used with an aim to preserve helical structure of the SRD. To determine if PKN3 can phosphorylate p130Cas in SRD domain we performed kinase assay in vitro with precipitated Strep-Flag-PKN3 and newly prepared GFP-p130Cas variants (WT, 15AN, S432A) in the presence of ATPγS followed by detection with specific antibody anti-thiophosphate ester (Fig. 4E). GFP-p130Cas WT had the highest thiophosphorylation compared to GFP-p130Cas 15AN and Ser432 which were thiophosphorylated to similar extent. Partial thiophosphorylation of GFP-p130Cas 15AN indicates that PKN3 could phosphorylate p130Cas also outside SRD domain (Fig. 4A). Noteworthy, PKN3 autophosphorylation was also observed (Supplementary figure S2E). These results verified the presence of PKN3 phosphorylation motif in the sequence surrounding Ser432 and indicated that PKN3 phosphorylates p130Cas on Ser432 in vitro.

Protein p130Cas similarly to Nedd9 (other member of p130Cas family; HEF1) exists in cells in two main isoforms which are attributed to different Ser/Thr phosphorylations (Hivert, Pierre and Raingeaud, 2009; Makkinje *et al.*, 2009). Depending on the cell type, p130Cas protein is present at SDS-PAGE as a single protein or detected as a doublet and the increased proportional representation of the upper band correlates with cell aggressive properties (Makkinje *et al.*, 2009; Janoštiak *et al.*, 2011). To test the biological relevance of p130Cas Ser432 phosphorylation in cells, we prepared lysates from p130Cas-/- MEFs with reintroduced GFP-p130Cas mutants with or without overexpressing mCherry-PKN3 WT and examined p130Cas migration profile after separation on SDS-PAGE using an acrylamide/bisacrylamide ratio of 30:0.2 (Fig. 4F) which improves the separation of Ser/Thr phosphorylation-induced gel shifts similarly as in (Hivert, Pierre and Raingeaud, 2009). GFP-p130Cas WT migrated as 4 bands with the most pronounced form which migrated the slowest. GFP-p130Cas Y12E displayed shift of the p130Cas protein content from the slowest migrating band towards to faster migration forms. 15 Ser/Thr mutations (15AN) migrated only in form of two faster bands similarly to single mutation of Ser432 (S432A mutant) and that was not changed by PKN3 overexpression (see Fig. 4F). Furthermore, GFP-p130Cas without CCH domain also migrated in form of two faster bands. We concluded that p130Cas SH3 and CCH domain are important for p130Cas Ser/Thr phosphorylation and the presence of the slowest migration form of p130Cas is associated with Ser432 phosphorylation. However, we failed to promote switch of slower migrating p130Cas (WT) isoform to faster ones by serum starvation (see again Fig. 4F) or by keeping cells in suspension (Supplementary figure S2F) and therefore we could not demonstrate the change of p130Cas WT SDS-PAGE migration pattern by PKN3 overexpression.

PKN3 overexpression regulates growth of MEFs and this effect requires PKN3 – p130Cas interaction

Both PKN3 and p130Cas have been implicated in regulating malignant cell growth (Leenders *et al.*, 2004; Cabodi *et al.*, 2006; Cabodi, Tinnirello, *et al.*, 2010). Although PKN3 is scarce in normal human adult tissues except in endothelial cells (HUVEC) (Aleku *et al.*, 2008) recent paper showed that PKN3 is also present in moderate levels in MEFs, making them to be physiologically relevant model (Mukai *et al.*, 2016). To investigate if PKN3 regulates cell proliferation in MEFs and if it is dependent on p130Cas, we prepared stable MEF cells with Dox inducible mCherry fused PKN3 WT or mCherry alone in the p130Cas null background with or without re-expression of p130Cas (Fig. 5A). mCherry-PKN3 WT expression started from 5 hours and reached saturation within 24 hours post treatment by doxycycline (Fig. 5B). Cell morphology was unaffected by mCherry-PKN3 WT expression but starting 5 hours after adding doxycycline MEFs re-expressing p130Cas increased growth rate compared to non-induced control (Fig. 5C). Induction of mCherry alone as an additional control didn't have any effect and the growth rate of p130Cas-/- MEFs was not affected by PKN3 expression (Fig. 5D-E), indicating that PKN3-mediated regulation of cell growth is p130Cas-dependent.

To investigate if PKN3-mediated induction of cell growth rate requires PKN3 interaction with p130Cas, we prepared stable cell lines of MEFs p130Cas-/- re-expressing p130Cas with doxycycline

inducible Flag fused PKN3 variants (WT, mPR, KD) (Fig. 5F). Only the induction of expression of PKN3 WT, but not mPR or KD, led to the increase of cell growth compared to non-induced controls (Fig. 5G). Increase of cell proliferation induced by PKN3 variants was also verified by Alamar blue assay (Supplementary figure S3A) with similar outcome.

To test if PKN3 promotes cell growth of MEFs by phosphorylation p130Cas SRD domain, we reintroduced GFP-p130Cas variants (WT, 15AN) or GFP as control to p130Cas-/- MEFs with dox-inducible mCherry-PKN3 (Supplementary figure S3B). Both GFP-p130Cas WT and 15AN, but not GFP alone, changed cell morphology characterized by increased number of cell protrusions (Supplementary figure S3C). This morphology was not changed by dox-inducible mCherry-PKN3, but doxycycline treatment increased cell growth of cells expressing GFP-p130Cas WT and 15AN compared to non-induced control (Supplementary figure S3D). Therefore, the effect of PKN3 on cell growth is probably independent of p130Cas SRD domain phosphorylation.

To investigate which signaling pathways are involved in the accelerated cell growth induced by PKN3, we analyzed activation status of STAT3, ERK, Akt, MLC, mTOR and Src signaling (Supplementary figure S4A). In agreement with previous studies we did not find any significant changes (Leenders *et al.*, 2004). Only Src activity was slightly increased by PKN3 expression in p130Cas dependent manner that is consistent with recent study demonstrating PKN3 to promote Src activity in osteoclasts (Supplementary figure S4A-B) (Uehara *et al.*, 2017).

Taken together, these results indicate that PKN3 regulates growth of MEFs and this effect requires PKN3-p130Cas interaction independently of p130Cas SRD domain phosphorylation.

The interaction of p130Cas with PKN3 is required for PKN3-dependent increase of invasiveness

The localization of PKN3 in lamellipodia suggests its importance in cell migration. In p130Cas-/- MEFs re-expressing p130Cas we analyzed the effect of inducible expression of PKN3 on 2D migration using a wound healing assay. We found that PKN3 expression has no effect on the 2D migration both on plastic or fibronectin (FN) (Fig. 6A-B). These results are consistent with study of Lachmann et al., (Lachmann *et al.*, 2011) where only siRNA anti-PKN1 or anti-PKN2, and not anti-PKN3, had an effect on wound healing closure of 5637 bladder tumor cells.

Next, we investigated the potential role of PKN3 for invasive cell migration in 3D collagen. To analyze the effect of PKN3 on cell invasiveness we utilized a 3D cell-zone exclusion assay as characterized in (Van Troys *et al.*, 2018). In this assay, a monolayer of the cells grown on thick layer of collagen is wounded and then the system is overlaid with another layer of collagen. The cells migrating into the wound adopts morphology and mechanisms of movement of cells migrating in 3D but can be monitored in one focal plane and their movement can be easily tracked and analyzed as in 2D (details described in methods). MEFs p130Cas-/- re-expressing p130Cas moved clearly faster and more individually compared to MEFs p130Cas-/- (Fig. 6C-D; supplementary movie S4 versus S5). Induced expression of PKN3 in p130Cas-/- MEFs (Fig. 6C-D, supplementary movie S5) was not sufficient to increase cell migration or to promote individual cell movement. In contrast, activation of PKN3 expression in MEFs p130Cas-/- re-expressing p130Cas leads to an increase of cell speed and invading distance compared to non-induced cells but did not change cell directionality (Fig. 6C-E, supplementary movie S4). Interestingly, induced expression of PKN3 mPR and KD variants did not induced invasiveness of p130Cas-/- MEFs re-expressing p130Cas (Fig. 6F-G) and in fact had the opposite effect suggesting that PKN3-p130Cas interaction and PKN3 activity is important for PKN3-induced cell invasiveness of MEFs in collagen.

To test if PKN3 promotes invasiveness of MEFs by phosphorylation of p130Cas SRD domain, we performed the 3D cell-zone exclusion assay with p130Cas-/- MEFs re-expressing GFP-p130Cas variants (WT, 15AN) or GFP as control with or without doxycycline to induce mCherry-PKN3. Re-expression of GFP-p130Cas (WT or 15AN) caused increase of cell invasive capability in 3D collagen (Supplementary figure S4C). Cell treatment by doxycycline further slightly increased migration velocity of cells re-expressing both GFP-p130Cas WT and GFP-p130Cas 15AN in collagen compared to non-induced controls (Supplementary figure S4C-D) indicating that phosphorylation of p130Cas in SRD domain by PKN3 is not involved in PKN3 dependent increase of MEFs invasiveness.

Taken together, our results suggest that PKN3 expression increases cell invasiveness of MEFs and this induced invasiveness is dependent on p130Cas. Furthermore, the PKN3 activity and its ability

to interact with p130Cas is required for PKN3-induced cell invasiveness of MEFs, but it is independent of PKN3-mediated phosphorylation of p130Cas SRD domain.

PKN3 regulates growth and invasiveness of Src-transformed MEFs in 3D environment through interaction with p130Cas

Having established the importance of the PKN3 – p130Cas interaction for cell proliferation and cell migration in 3D environment, we next analyzed whether this interaction also influences the growth and invasive behavior of SrcF-transformed cells. We first analyzed the effect of SrcF-induced transformation on the level of endogenous PKN3. We found that PKN3 expression is significantly increased in MEFs transformed by activated Src (almost 2x; $p<0,009$) and that this increase is dependent on presence of p130Cas (Fig. 7A, Supplementary figure S5A). To reduce the contribution of endogenous PKN3 in subsequent experiments, we inactivated PKN3 in SrcF MEFs p130Cas-/- re-expressing p130Cas (SC cells) using CRISPR/CAS9 system (see methods; Fig. 7B). All PKN3 KO clones (SCpkn3-/-) tested had significantly reduced proliferation compared to the parental cells (Fig. 7C). Consistently, reintroduction of PKN3 (mCherry-Flag fused), but not PKN3 mPR or mCherry alone, under doxycycline-controlled promotor (Fig. 7D) led to rescue of cell growth in SCpkn3-/- cells when Dox was supplemented to the medium (Fig. 7E, Supplementary figure S5B).

To mimic the tumor environment, we further examined the growth of SCpkn3-/- cell lines in 3D environment similarly as in (Unsal-Kacmaz et al., 2012). Induced expression of PKN3 in the SCpkn3-/- promoted a more aggressive behavior characterized by appearance of larger number of multicellular clusters in 3D Matrigel when compared to uninduced cells (Fig. 7F-G). In contrast, inducible expression of PKN3 mPR did not significantly changed cell growth. To further confirm our results that PKN3 supports aggressive cell behavior of SrcF-transformed MEFs in Matrigel, we also established stable SC cell line inducibly expressing shRNA anti-endogenous PKN3 (Fig. 7F-H). Consistently, the enhanced growth of parental SC cells compared to SCpkn3-/- cells was reduced by doxycycline induced shRNA anti-PKN3 to a basal level of SCpkn3-/-cells (Fig. 7G). Taken together, these results suggest that PKN3 supports a more malignant phenotype in SrcF MEFs and that interaction PKN3 with p130Cas could at least partly mediate this effect.

p130Cas has been previously shown to be crucial for invasion of SrcF-transformed MEFs (Brábek *et al.*, 2004). To investigate if PKN3 can influence migration of SrcF-transformed MEFs in 3D environment we used the 3D cell-zone exclusion assay. In agreement with the results obtained in untransformed MEFs, in SCpkn3-/- cells induction of PKN3 expression, and not PKN3 mPR, led to an increase of cell invasion (Fig. 8A-B). Consistently, inducible downregulation of PKN3 in parental SC cells by shRNA led to decrease of cell migration in collagen (Fig. 8A-B).

p130Cas and Src are critical components of podosome-like structures, involved in degradation of ECM (Brábek *et al.*, 2004). We further showed that PKN3 is also localized to podosome-like structures. Therefore, we next tested whether the increased invasiveness of PKN3 overexpressing cells is due to their elevated ECM degradation activity. We analyzed the podosome-associated proteolytic activity by gelatin degradation assay and found that gelatin degradation in SCpkn3-/- cells is not affected by expression of PKN3 (Fig. 8C). These results indicate that induced invasiveness of SCpkn3-/- cells expressing PKN3 reflects rather PKN3-induced migratory phenotype than increased degradation of ECM.

Nevertheless, PKN3 was recently demonstrated to be necessary for bone degradation/resorption activity of osteoclasts similarly as published for p130Cas (Nagai *et al.*, 2013; Uehara *et al.*, 2017). In both cases was required intact polyproline sequence of PKN3 and p130Cas SH3 domain, we validated for PKN3-p130Cas binding, and both sequences were implicated in osteoclast function through an association with Src. We hypothesized that Src-PKN3 interaction is indirect and mediated by p130Cas and tested this by co-immunoprecipitation experiments from SrcF-transformed MEFs p130Cas-/- with or without p130Cas re-expression. Indeed, we found that Src failed to co-precipitate with PKN3 in absence of p130Cas, confirming that Src-PKN3 interaction is indirect (Fig. 8D).

The interaction of p130Cas with PKN3 is required for PKN3 dependent tumor growth in vivo

Independent studies have shown that both PKN3 and p130Cas enhance cell proliferation in vitro and can contribute to various stages of tumor development in vivo ((Leenders *et al.*, 2004; Unsal-Kacmaz *et al.*, 2011; Tornillo, Defilippi and Cabodi, 2014); see introduction).

To expand our results that show functional relevance of interaction between PKN3 and p130Cas in vitro to in vivo analysis we subcutaneously injected SCpkn3-/- cells stably engineered for inducible expression of either PKN3 WT or PKN3 mPR fused to mChery or mCherry alone to nu/nu mice (total 48). As positive control a parental line of SC cells inducibly expressing mCherry was used. The animals were split into four groups (12 per group), all treated with Dox to induce the expression of mCherry fused PKN3 variants or mCherry alone. The primary tumors were surgically removed; in the SCpkn3-/- cell lines in days 21 (+PKN3 WT, +mCherry) and 22 (+PKN3 mPR) after inoculation, in parental SC cells inducibly expressing mCherry due to large tumor sizes already at day 16 (Fig. 8E-F). The tumors from parental SC cells with inducible mCherry despite the shorter period of time reached the highest weight. The SCpkn3-/- cells expressing mCherry induced the smallest tumors among all groups. Re-expression of PKN3 WT, but not PKN3 mpR in SCpkn3-/- cells have led to significant increase of tumors weight when compared to SCpkn3-/- (Fig. 8C-D). Despite that the tumors from SCpkn3-/- re-expressing PKN3 mPR were removed one day later than SCpkn3-/- re-expressing PKN3 WT their comparison by statistical analysis (ANOVA on ranks, Tukey's post hoc test) gives almost significant p value 0.059 indicating that PKN3 promotes tumor growth from SCpkn3-/- cells and that PKN3 – p130Cas interaction could be important in this promotion.

We further analyzed individual tumors for expression of mCherry as a reporter for Dox induced expression in the tumor cells using a dot blot analysis (Supplementary figure S5C). Despite the comparable PKN3 mPR and WT protein level produced by Dox-induced cells in vitro, most of the mCherry-PKN3 mPR expressing tumors had surprisingly significantly increased mCherry signal compared to tumors with mCherry-PKN3 WT. This increase, however, did not lead to comparable tumor growth.

Since both p130Cas (Brábek *et al.*, 2005) and PKN3 (Unsal-Kacmaz *et al.*, 2011) expression are able to promote metastasis, we also evaluated of the presence of lung metastases after 14 days post-surgery in animals injected with the parental SC cells, and 21 days in all SCpkn3-/- cells (schematic representation of the experiment in Supplementary figure 5D). Metastases were observed clearly only in 3 out of 5 survived mice injected with parental line of SC cells (Supplementary figure S5E) suggesting that 21 days post-surgery (total 42 days) was not sufficient time period for formation of detectable metastases in mice injected with SCpkn3-/- cells.

Discussion:

In this study, we have, for the first time, shown and characterized PKN3-p130Cas interaction and provided a new insight into the molecular mechanism of regulation of tumor-promoting kinase PKN3 and p130Cas-mediated signaling. We demonstrated that PKN3-p130Cas interaction is necessary for PKN3 to promote malignant growth and invasiveness of SrcF-transformed MEFs.

The interaction between mouse p130Cas and mouse PKN3 is mediated by binding of p130Cas SH3 domain and PKN3 central polyproline region (P_{500}PPKPPRL; Fig. 1A-F). The dynamics of this interaction is potentially regulated similarly as other p130Cas SH3 ligands by Src-dependent phosphorylation of p130Cas SH3 domain on Tyr12 which in non-phosphorylated state contributes significantly to p130Cas SH3 ligand binding (Gemperle *et al.*, 2017).

PKN3-p130Cas interaction represents new crosstalk of PI3K – integrin signaling. p130Cas was previously shown to be in complex with PI3K to support cell growth resistant to anti-estrogenic drugs (Cabodi *et al.*, 2004). The connection of PKN3 to integrin signaling is indicated by study showing that PKN3 knockout decreased chemotaxis of MEFs towards fibronectin and caused a glycosylation defect of integrin β1 and integrin α5 (Mukai *et al.*, 2016). Moreover, PKN3 promotes osteoclasts to resorb bone matrix via stimulation of integrin effector kinase - Src kinase (Uehara *et al.*, 2017). This effect was strongly dependent on PKN3 polyproline region we showed to be responsible for p130Cas binding. We were able to demonstrate that PKN3-Src association is indeed mediated by p130Cas (Fig. 8D). Furthermore, consistently with osteoclasts, we observed slight activity increase of integrin effector kinase - Src kinase induced by PKN3 overexpression (Fig. 7A and Supplementary figure S4A-B).

We found PKN3 to co-localize with p130Cas in pro-invasive structures: lamellipodia of MEFs and podosome rosettes of Src-transformed MEFs (Fig. 2A-B). Remarkably, PKN3 was not detected at focal adhesions which are highly redundant in terms of protein composition with podosome rosettes, while p130Cas is present in both structures. Since PKN family kinases are implicated in cell migration, we investigated the role of PKN3 in cell migration and invasiveness. MEFs migration measured by wound healing assay (2D) was not affected by PKN3 overexpression (Fig. 6A-B). In contrast, we observed increased cell velocity in collagen (3D) upon induction of PKN3 expression, but not kinase inactive PKN3 variant (KD) nor PKN3 variant unable to bind p130Cas (mPR). Importantly, the effect of PKN3 expression on migration in 3D was dependent on p130Cas expression (Fig. 6C-G; 8A-B). Our results are consistent with independent studies where the invasiveness of SrcF-transformed MEFs through Matrigel was greatly decreased in the absence of p130Cas (Brábek *et al.*, 2005) and where MEFs PKN3 KO cells exhibited lower migratory activity induced by various treatments than MEFs with endogenous PKN3 (Mukai *et al.*, 2016). Similarly, Leenders et al 2004 indicated that PC3 cells with downregulated PKN3 had failed to migrate to form network-like structures on Matrigel (Leenders *et al.*, 2004). Although we have not elucidated the exact molecular mechanisms how PKN3 promotes cell migration, we observed PKN3 binding to actin in p130Cas dependent manner (Supplementary figure S5F) and temporal colocalization of PKN3 with stress fibers (Fig. 3A and Supplementary figure S1BC). Given the binding of PKN3 also to regulators of actin dynamics - Rho GTPases (Unsal-Kacmaz *et al.*, 2011) we predict that PKN3 is affecting intracellular actin dynamics and p130Cas is involved.

PKN3 is the first kinase documented to phosphorylate p130Cas on Ser/Thr residues (Fig. 4E) which are abundantly present on p130Cas and exert dynamic phosphorylation pattern (Makkinje *et al.*, 2009). One of these residues of p130Cas is Ser432 (homologous to human 428) which is abundantly phosphorylated in breast carcinoma tumors (Fig. 4D) and represents one of the major Ser/Thr phosphorylation sites in MEFs cultivated in vitro (Fig. 4F). Notable, some of phosphoproteomic studies show that this phosphorylation is enriched in response to insulin which is potent activator also for PKN3 (PhosphoSite database, (Leenders *et al.*, 2004)) and in breast carcinoma tumors correlates with PKN3 activity (Fig. 4D). The effect of this phosphorylation and phosphorylation of p130Cas in SRD domain is still unknown as p130Cas-/- MEFs with reintroduced GFP-p130Cas 15AN increased cell growth and invasiveness similarly as GFP-p130Cas WT in PKN3 dependent manner (Supplementary figure S3D, S4C-D).

Interestingly, p130Cas paralog called Nedd9 was found to be phosphorylated on Ser369 homologous to p130Cas Ser432. Mutation of Ser369 to alanine similarly as mutation of p130Cas Ser432 induces p130Cas mobility shift at SDS-PAGE from 4 bands to two faster migrating bands (Hivert, Pierre and Raingeaud, 2009). A kinase responsible for Nedd9 Ser369 phosphorylation is unknown but the phosphorylation was shown to induce Nedd9 proteasomal degradation. Protein p130Cas, however, is stable during cell cycle and exhibit constant expression pattern in cells. Therefore, the effect of p130Cas Ser432 phosphorylation is different from that of Ser369 in Nedd9.

Interestingly, transformation of MEFs by constitutive active Src have led to an increase of PKN3 endogenous protein levels in cells grown on plastic. This increase of PKN3 level in cells was dependent on presence of p130Cas (Fig. 7A, Supplementary figure S5A). Similarly, PKN3 levels were shown to be elevated by its activators PI3K (Leenders *et al.*, 2004), RhoA/C (Unsal-Kacmaz *et al.*, 2011) and by oncogenic form of Ras (Leenders *et al.*, 2004). This suggests that PKN3 is an effector of various signal transduction pathways that mediate cell growth and transformation.

Several studies presented evidence for significant contribution of PKN3 and p130Cas to tumor growth and also metastasis formation (Leenders *et al.*, 2004; Brábek *et al.*, 2005; Unsal-Kacmaz *et al.*, 2011; Tornillo, Defilippi and Cabodi, 2014; Kang *et al.*, 2015). Our data support these results and furthermore suggest that binding of PKN3 to p130Cas is important for PKN3-induced tumor growth. We hypothesize that targeting p130Cas, PKN3 and their co-operation could be exploited in cancer therapy and based on our insight in PKN3 signaling in osteoclasts also in pathophysiological signaling related to bone disease such as osteoporosis, rheumatoid arthritis, and periodontal disease. It is noteworthy that therapeutic agent that targets PKN3 by RNA interference (siRNA Atu027) has already finished Phase I clinical trials (study with patients with different solid advanced and metastatic tumors) with very promising results without any adversary effects (Schultheis *et al.*, 2014).

Material and methods

Antibodies and reagents

The following antibodies were used: Akt (rabbit pAb, #9272S), phospho-Akt (Ser473, rabbit mAb D9E, #4060S), phospho-p130Cas (Tyr165, rabbit pAb), p44/42 MAPK (=Erk1/2, rabbit mAb 137F5, #4695), phospho-Src family (Tyr416, rabbit pAb, #2101S), Stat3 (rabbit mAb D3Z2G, #12640), Phospho-Stat3 (Tyr705, mouse mAb 3E2, #9138S), Phospho-Myosin Light Chain 2 (Ser19, mouse mAb, #3675), Phospho-S6 Ribosomal Protein (Ser235/236, rabbit mAb 2F9, #4856), Phospho-GSK-3α/β (Ser21/9, Rabbit mAb 37F11, #9327) antibody (Cell Signalling Technology); p130Cas (mouse mAb 24), Paxillin (mAb 349) antibody (BD Transduction Laboratories); Src (Calbiochem, mouse mAb 327, Ab–1); FAK (rabbit pAb, C–20), Actin (goat pAb, C–11) antibody (Santa Cruz Biotechnology); MAPK (=Erk1/2, mouse mAb V114A, Promega); GST (rabbit pAb, G7781, Sigma Aldrich); PKN3 (rabbit pAb, NBP-130102), mCherry (rabbit pAb, NBP2-25157), StrepII (mAb 517, NBP2-43735) antibody (NOVUS biologicals); PKN3 (rabbit pAb, AP14628A, Abgent); phospho-PKN3 (human Thr860 = mouse Thr849) antibody was obtained from (Pfizer, Oncology, Pearl River). Immunoprecipitations were carried out using Flag antibody (mouse mAb M2, Sigma Aldrich); GFP antibody (Abcam, rabbit polyclonal ab290). Secondary antibodies fused to HRP (Abcam) were used as recommended by the manufacturer. The secondary antibodies for fluorescent imaging were: anti-rabbit (Alexa-546), anti-mouse (Alexa-594, Alexa-633; Molecular Probes).
The reagents used were doxycycline hydrochloride, blasticidin and puromycin (Sigma Aldrich), Glutathione (reduced, LOBA Chemie), Phalloidin 405 (Thermo Fisher Scientific), Fibronectin (Invitrogen), Collagen R solution (SERVA), Matrigel (Corning), Strep-Tactin® Superflow® resin (IBA Lifesciences), nProtein A Sepharose 4 Fast Flow (GE Healthcare), anti-Flag M2 affinity resin (Sigma), p-Nitrobensyl mesylate (Abcam)

Cell lines and culture conditions (shRNAs, transfection, retrovirus, lentivirus preparation)

p130Cas-/- MEFs were obtained from Steven Hanks (Vanderbilt University, Nashville). p130Cas-/- MEFs expressing constitutively active mouse Src Y527F (SrcF cells) or both p130Cas WT and Y527F (SC cells) were prepared using the LZRS-MS-IRES-GFP retroviral vector and the Phoenix E packaging line as described previously (Brábek *et al.*, 2004).
To generate SC PKN3 null, cells were transiently transfected by sgRNA anti-PKN3 (sequence in Table S2) and puromycin resistance expressing CRISP-CAS9 plasmid. Cells were selected by puromycin for 2-3 days followed by clonal isolation. Success of CRISPR targeting was analyzed by PCR and Surveyor nuclease assay as published (Ran *et al.*, 2013) and by western blots. Sequences around CRISPR modification site were amplified by PCR from 3 selected mammalian clones, cloned to pJET1.2/blunt by CloneJET PCR Cloning Kit (ThermoFisher) and sequenced (at least six from each). Sequenation revealed that CRISPR nicking caused most often frameshift -1bp or + 49/+37bp. Potential offtargets were predicted (http://tools.genome-engineering.org) and 3 most potent tested by Surveyor assay (results negative, primer sequences provided in the Table S2). SC cells with dox-inducible PKN3 shRNA (see plasmid construction section) were prepared similarly as described previously (Czauderna *et al.*, 2003; Leenders *et al.*, 2004).
To stably deliver Flag fused or mCherry-Flag fused constructs, retroviral pMSCV-puro or lentiviral pLVX-Tet-On Advanced system (Clontech) was used. Shortly: Cells were infected with viral supernatant generated in transfected Phoenix E packaging cells (pMSCV system) or produced in HEK293T co-transfected by pVSV-G and psPAX2 plasmids together with pLVX-Tet-On in first round or with pLVX-tight-puro in the second. All cells were then selected with puromycin (2,5 ug/ml) or/and blasticidin (2-4 ug/ml) and alternatively sorted by FACS (1-3 rounds) after transient (24 h) induced expression by doxycycline. Cells without fluorescent protein were cloned and tested by western blot. SCpkn3-/- cells from clone 1 were used for reintroduction of PKN3 (mCherry-Flag fused constructs).
To re-introduce GFP fused p130Cas variants to p130Cas-/- MEFs, a retroviral pBabe system was used. After infection of p130Cas-/- MEFs by viral supernatants prepared in HEK293T cells co-transfected by pVSV-G, Gag-Pol and pBabe respective plasmids, GFP positive cells were selected by FACS sorting.

MDA-MB-231 cells were provided by Dr. Marie Zadinova from Charles University. All transfections were carried out according to the manufacturer's protocol using Jet Prime (Polyplus Transfection) or PEI transfection reagent (Polysciences). All cells were cultivated in full DMEM (Sigma) with 4.5 g/l L-glucose, L-glutamine, and pyruvate, supplemented with 10% fetal bovine serum (Sigma) and ciprofloxacin (0.01 mg/ml) at 37 °C and 5% CO2. Cells were tested for mycoplasma contamination.

Plasmid constructions

cDNAs coding for p130Cas SRD domain variants (WT, 15AN; sequences provided in the Table S1) were commercially synthesized and cloned into pMA-T vector (geneArt, Life technologies). 15AN variant was generated by mutation of all 15 Ser/Thr to Ala or Asn. Mutant variant S432A (KRLS to KRLA) was created later by whole plasmid synthesis using Q5 polymerase (New England Biolabs) and respective site-directed mutagenesis primers (listed in the Table S2). Aſter PCR, 5U of DpnI were added to each reaction and incubated for 1.5 h at 37 °C. Individual mutated clones were screened by sequencing. Sequences of all SRD variants were then switched with original p130Cas SRD domain cassette within p130Cas sequence (pUC19 vector) using Bpu10I/SacII sites. pEGFP-C1 p130Cas variants and pGEX-p130Cas-SH3 domain constructs were prepared similarly as described previously (Janoštiak *et al.*, 2011; Braniš *et al.*, 2017). GFP-fused p130Cas variants were introduced into pBABE retroviral expression vector by EcoRI and blunt end (generated by BamHI/AgeI restriction followed by fill in by Klenow). All constructs were verified by sequencing. To prepare GSK3-derived peptide fused to GST a pair of phosphorylated oligonucleotides (see Table S2) was annealed and inserted in frame at the 3′ end of the GST (pGEX vector) using BamHI/EcoRI sites. Production of GST fused proteins (SH3, GSK3) from pGEX system were carried out as in (Gemperle *et al.*, 2017). Oligos for sgRNA construction and primers for CRISPR offtarget screening were designed and plasmids constructed (LentiCRISPR, BsmBI site) as published (Ran *et al.*, 2013) and are listed in the Table S2. PKN3 shRNA was cloned into a lentivirus-adapted vector system allowing Dox-inducible expression of shRNAs (Czauderna *et al.*, 2003) via PCR followed by ligation and DpnI mediated cleavage of template DNA. Primers are listed in the Table S2. Correct insertion of the shRNA sequence was confirmed first by restriction analysis, confirming reintroduced BsrgI restriction site and then with DNA sequence analysis.

cDNAs coding for whole mouse PKN3 with added sequence for Flag epitope and shorter sequence with mutations to create mPR and KD variants (sequences provided in the Table S1) were commercially synthesized and cloned into pMK-RQ or in pMA-T vectors, respectively (geneArt, Life technologies). mPR mutant was created to abrogate binding to p130Cas (motif P_{500}PPKPPR to PAPSAPR) similarly as suggested in (Gemperle *et al.*, 2017). KD mutation was designed as published for human PKN3 (Leenders *et al.*, 2004). Sequence for mPR was swapped within whole PKN3 in pMK-RQ vector by NdeI/HindIII sites, KD by NdeI/BamHI followed by cloning PKN3 variants (WT, mPR, KD) to corresponding other vectors: mCherryC1/eGFP C1 (BsrgI/EcoRI), pMSCV-Puro (XhoI/EcoRI), pLVX-Tight-Puro (BsrgI/EcoRI). Lentiviral expression vector pLVX-Tight-Puro allowing Dox-inducible gene expression was also prepared with mCherry fused PKN3 variants via NheI/EcoRI and XbaI/EcoRI sites. Flag-fused mCherry control was prepared similarly, except prior to cloning to pLVX-Tight-Puro system sequence of Flag was inserted in frame in front of mCherry in mCherry C1 vector by annealing the phosphorylated oligonucleotides described in the Table S2 and digested NheI/HindIII vector sites. Prior to kinase reactions in vitro, Flag-PKN3 was also cloned to StrepII pcDNA3 vector over blunt end ligation (AfeI/EcoRV vector sites, Flag-PKN3 cleaved from pMSCV-puro by BsrgI/EcorI and fill in by Klenow). CFP or mCherry-fused LifeAct was prepared as published (Riedl *et al.*, 2008). All constructs were verified first by restriction analysis and then by sequencing.

Preparation of cell extracts and immunoblotting

Cell were lysed in RIPA (total lysates; composition: 150 mM NaCl; 50 mM Tris-HCl, pH 7.4, 1 % Nonidet P-40, 0.1 % SDS, 1 % sodium deoxycholate, 5 mM EDTA, 50 mM NaF) or in 1% Triton lysis buffer (immunoprecipitations, pull downs; composition: 50 mM Tris HCl [pH 7.1], with 150 mM NaCl and 1% TRITON X–100) supplemented with protease (MixM; SERVA) and phosphatase inhibitors (MixII; SERVA) followed by immunoblotting as described previously (Janoštiak *et al.*, 2014). Shortly: Protein extracts were separated using SDS-PAGE under denaturing conditions (6–

15% gels) and were transferred to the nitrocellulose membrane (Bio-Rad Laboratories). Membranes were blocked with 4% BSA or 3% milk-TBST (Tris-buffered saline and 0.05% Tween 20), incubated with the indicated primary antibodies overnight at 4°C, and then incubated with HRP-linked secondary antibodies at RT for 1 h, washed extensively in TBST, and developed using an AI600 System (GE Healthcare). To improve the separation of p130Cas by SDS-PAGE a ratio of acrylamide/bisacrylamide 30:0.2 was used.
Immunoprecipitations (see kinase assays section), Pull-downs and Far western experiments were carried out similarly as in (Gemperle et al., 2017 and Janoštiak et al., 2014). For far-Western-blot analysis, the protein blots were incubated with 2 µg/ml recombinant human GST-p130Cas/BCAR1 (Abcam) or purified mouse GST-p130Cas SH3 diluted in 1% BSA in TBST overnight followed by washing with TBST and incubation (2 h, 4 °C) with anti-GST antibody (Sigma). After extensive washing with TBST, blots were treated with HRP-conjugated secondary antibodies and developed using the AI600 System.
Band intensity was determined using Fiji (ImageJ; National Institutes of Health; Schindelin *et al.*, 2012).

Kinase assays
Cells were transfected with either Flag- or StrepII-fused mouse PKN3 (WT or KD) using PEI transfection reagent (Polysciences) according to the manufacturer instructions. After 48h, cells were washed with PBS (phosphate-buffered saline) and lysed in standard lysis buffer (50mM Tris-HCl [pH 7.1], 150mM NaCl, 1% Triton-X-100) with protease and phosphatase inhibitors (SERVA) and 10mM Glycerol-2-Phosphate (Sigma). Proteins were immunoprecipitated with anti-Flag M2 affinity resin (Sigma) and eluted with Flag peptide as described previously (Unsal-Kacmaz *et al.*, 2011). StrepII-fused PKN3 was precipitated with Strep-Tactin® Superflow® resin (IBA Lifesciences) and eluted with 1x Buffer E (Strep-Tactin Elution Buffer, IBA Lifesciences). Kinase assays were carried out in conditions described previously (Leenders *et al.*, 2004; Unsal-Kacmaz *et al.*, 2011). GFP-fused p130Cas variants (WT, 15AN, S432A (see plasmid constructions section)) were immunoprecipitated from transiently transfected cells using anti-GFP 3E6 antibody (Invitrogen) and nProtein A Sepharose 4 Fast Flow (GE Healthcare). Subsequently, immobilized p130Cas was dephosphorylated using Lambda protein phosphatase (New England Biolabs) as specified by manufacturer. Phosphatase was inactivated by two washes with TBS containing 10mM Sodium Orthovanadate and 20mM EDTA and two washes with TBS and p130Cas variants were eluted with 0,1M Glycine pH 3.5 for 10min in RT. After elution pH was equilibrated by adding corresponding volume of 1M Tris pH 9.2 and proteins were used as a substrate in reaction with 1mM ATPγS (Sigma). After 45 minutes in 35°C, reactions were stopped with EDTA to a final concentration of 20mM and alkylated with 50mM p-Nitrobensyl mesylate (Abcam) at RT for 2 h. Samples were resolved using SDS-PAGE and immunoblotted using anti-thiophosphate ester antibody (clone 51-8, Abcam). GSK3-derived peptide fused to GST was prepared and used as a positive control for PKN3 activity as described previously (Unsal-Kacmaz *et al.*, 2011) and its phosphorylation detected by anti-Phospho-GSK-3α/β antibody. For autoradiography, kinase reactions were performed similarly, with 5µCi [γ-32P] ATP added to the reaction. The samples were heated 10min at 95°C, resolved using SDS-PAGE and subjected to autoradiography.

2D and 3D migration assays
Scratch-based migration assays in 2D were carried out using an IncuCyte automated imaging system (Essen BioScience). Briefly, MEFs with Dox-inducible PKN3 WT were seeded onto 96-well plates (Corning) at a density of 100,000 cells/well (10% serum in DMEM) and half of wells supplemented with doxycycline (final 250 ng/ml). After 24h monolayers of cells were scratched using a scratching apparatus that produced strongly identical scratches in each well. The IncuCyte system was programmed to obtain real-time phase-contrast images of the wounds every 2 hours for 2 days. Cell migration was automatically quantified and expressed as relative wound density, which indicates the ratio of sharpness of the wounded area and of the adjacent non-wounded area. The IncuCyte imaging system was then used to automatically calculate the area of each wound at each time point up to the point of complete closure of the wound from an average of the quadruplicate.

3D cell zone exclusion assays were carried out with JuLI™ Br (NanoEnTek) system with 2 microscopes situated in the incubator. Collagen R solution (4 mg/ml, SERVA) was diluted to final mix: 1 mg/ml Collagen, 1 % serum (to decrease the effect of proliferation), 1 x DMEM, 15 mM HEPES (750 mM), 8,5 mM NaOH (1M), 0,4 % NaHCO3 (7,5 %, sigma) and 5 µg/ml folic acid. 40 µl of the collagen mix was then added into each well (total 6) of two 96 well plate and let to polymerize at 37 °C. 100 ul of cell suspension ($1x10^6$ cells/ml) non-induced or 24h Dox-preinduced cells was added on top of a collagen gel. After cell attachment (4 hours), medium was removed, and scratch was performed. Immediately after removal of the rest of media in the generated wound, another layer of collagen mix (100 ul) was added (schema of the experiment shown in (Van Troys *et al.*, 2018)). Collagen was let to polymerize 15 min at RT, to prevent formation of bubbles in the collagen interface, then another 15 min at 37 °C. Finally, 100 ul of DMEM medium with 1 % serum supplemented with or without doxycycline (500 ng/ml) was added on the top of each well and cell CellTracker software (Piccinini, Kiss and Horvath, 2015) was used to manually track at least 60 random (fastest) (top) migrating cells across the cell/collagen interface in the main focus plane from three independent replicates. To create cell migration/tracking maps the "Chemotaxis And Migration Tool" version 2.0 (Ibidi) was used.

2D proliferation and 3D cultures in Matrigel

To determine difference in cell proliferation capacity among individual clones AlamarBlue assay was used. 10 000 cells per well in 96 well plate was seeded and after cell attachment (4h) medium was removed and replaced by a culture medium solution containing 10 % AlamarBlue. The plates were further incubated for 2 h at 37 °C prior to initial cell mass measurement followed by replacing with standard medium (± Dox if required). Cell growth was than measured again after 72 h by a culture medium solution containing 10% AlamarBlue to assess the increment of cell mass. Absorbance was measured at 570 nm (with reference at 600 nm) using a microplate reader Infinite M200 PRO. As a control, AlamarBlue was added to the cell growth medium without cells. The assay was performed in triplicates and was repeated three times.

The xCELLigence RTCA technology that provides a highly standardized experimental conditions was used to study cell proliferation. The cells were counted (100 000/ml) and then separated to supplement one part with doxycycline (final 250 ng/ml), second part without. Afterwards 10 000 cells +/- doxycycline were seeded per well of xCELLigence E-plate in triplicates, 30 minutes left to sit in room temperature and then transferred to xCELLigence RTCA device. Data were collected every 30 minutes for 48-72 hours. All data were recorded using RTCA Software version 2.0 which generated curve-slope values reflecting speed of cell growth. Cell growth was calculated from the log growth phase of curve starting 4-9 hours post Dox-induction followed by processing in MS Excel and compared to non-induced controls. E-plates were recycled to get rid of cells and used repeatedly up to 3 times.

SC cells were embedded into Matrigel (Corning) as published before (Unsal-Kacmaz *et al.*, 2011). In brief, cells grown in 6 cm dishes with or without Dox for 24 h were detached from culture dishes and suspended in Matrigel solution (per well: 80 µl of Matrigel and 20 µl of medium with 10% serum and 20 000 cells) at 4 °C. 100 µl of this Matrigel embedded cell suspension was overlaid on a 40 µl of Matrigel in a 96-well plate. The plate was allowed to solidify at 37 °C in the incubator. After 30 min DMEM media ± Dox (500 ng/ml) was added and replaced every 2-3 days. After 7 days multicellular clusters were imaged using differential interference contrast (DIC) microscopy (Nikon-Eclipse TE2000-S) and analyzed from duplicated wells. Quantification was counted based on at least 3 independent experiments.

Microscopy and immunostaining

Confocal images/movies were acquired with Leica TCS SP2 or SP8 confocal microscope system equipped with Leica 63×/1.45 oil objective (two HyD detectors and two standard PMT detectors, Leica LAS-AF software) followed by processing in Fiji.

Cells were seeded on cover slips coated with human fibronectin 10 µg/ml (Invitrogen), grown for 24 to 48 h, and subsequently fixed in 4% paraformaldehyde, permeabilized in 0.5% TritonX-100, washed extensively with PBS, and blocked in 3% bovine serum albumin. The cells were then sequentially incubated with primary antibody (dilution according to manufacturer´s protocol) for 2 h, secondary

antibody for 60 min and Alexa Fluor 594 phalloidin (Molecular Probes) for 15 min, with extensive washing between each step. In addition, slides were mounted with Mowiol 4–88 (475904; EMD Millipore) containing 2.5% 1,4-diazobicyclo-[2.2.2]-octane (D27802; Sigma-Aldrich) in the presence or absence of DAPI for nuclear staining and imaged at RT.
Colocalization analyses of PKN3 with p130Cas and actin in lamellipodia were conducted on live cells co-transfected by mCherry-PKN3 variants (mPR, WT, -), GFP-p130Cas and CFP- fused LifeAct. Alternatively, GFP-PKN3 variants and mCherry-LifeAct were used. The cells were placed on glass-bottom dishes (MatTek, Ashland, MA, USA) coated with 10 µg/ml fibronectin, transfected and cultured for 24 h before the experiment. Movies were performed in DMEM without phenol red supplemented with 10 % Serum at 37 °C and 5 % CO2 by Leica TCS SP2 or SP8 confocal microscope (63×/1.45 oil objective). Quantification of mCherry-PKN3 WT, mCherry-PKN3 mPR and mCherry localization to lamellipodia (lifeActin as marker) was calculated by measuring signal ratio of mCherry fluorescence in lamellipodium versus in cytosol (5 um from lamellipodium). Total160 measurements (50 living cells) gathered in 3 independent experiments were performed using Fiji.
Gelatin degradation assay was performed according to the manufacturer instructions (QCM™ Gelatin Invadopodia Assay, Merck Millipore). Cells were seeded on gelatin supplemented with DMEM, 10 % serum +/- doxycycline and gelatin degradation was assessed 48 hours after by Nikon-Eclipse TE2000-S (10x/0.25 or 20x/0.40 Nikon objective) followed by processing in Fiji.
Lung metastases on the lung parenchyma were visualized by fluorescent macroscope Carl Zeiss AxioZoom.V16 followed by processing in Fiji.

Subcutaneous mouse tumor models

Nu/nu mice (total 48, n = 12 per group), 8-week old, were subcutaneously injected with 1 x 10^6 GFP-positive SC cells (200 ul of suspension in PBS) that either expressed endogenous PKN3 (group 1) or lacked PKN3 expression (group 2, 3 and 4). In these cells was expression of mCherry vector (group 1 and 2) or mCherry fused Flag-PKN3 WT (group 3) or mCherry fused Flag-PKN3 mPR (group 4) induced by doxycycline hydrochloride that was administered via doxycycline pellets 200 mg/kg at the day of cell injection. After 16 days tumors were surgically removed (group 1, faster tumor growth), 21-22 days within groups 2-4 respectively, and their weight was determined, which was followed by disruption by tissue tearor in RIPA lysis buffer containing protease inhibitors (Serva) and preclearance by centrifugation at 16 000 g at 4 °C for 30 min. Tissue lysates were normalized to GFP level (Infinite M200 PRO) and analyzed by immunoblotting (SDS-PAGE separated or DOT BLOT) as described in (Janoštiak *et al.*, 2014). Post operation was doxycycline hydrochloride administered via drinking water in concentration 0,2 mg/ml and supplemented with 1 % sucrose. Animals in group 1 were killed 14 days post-surgery, and in groups 2-4 21 days post-surgery, and their lungs were collected. Immediately at sacrifice right lungs were washed in PBS and viewed under a fluorescence microscope to analyse GFP and mCherry-positive metastases grown on the surface, as well as within the lung parenchyma. Right lungs were fixed 72h in 4 % PFA for immunohistochemistry analysis. All experiments (surgery, cell transplantation, measurement of tumor weight) were performed blinded and independently by two researchers, and in compliance with the guidelines of the Ministry of Education, Youth and Sports of CR (institutional approval no.70030/2013-MZE-17214).

In silico analysis

Data of invasive breast carcinoma (1100 tumors in TCGA, provisional) and prostate adenocarcinoma studies (499 tumors, TCGA, provisional) were retrieved from and analyzed using the cBio Cancer Genomics Portal (cbioportal.org) (Gao *et al.*, 2013) or processed by the SigmaPlot software package (Systat Software, Inc., Point Richmond, CA). The available data on protein phosphorylation levels of p130Cas/BCAR1 were renumbered from isoform 6 (Ser474) to isoform 1 (corresponding Ser432)

Statistical analysis

Statistical analyses were done using the SigmaPlot software package (Systat Software, Inc., Point Richmond, CA). Data with a normal distribution were subjected to one-way ANOVA, whereas data failing the normality test were analyzed by one-way ANOVA on ranks followed by Dunn's post hoc comparison. All compared groups passed an equal variance test. Where not indicated differently, same cells treated or not treated by doxycycline are compared. Graphs were created using Graphpad Prism 6

(San Diego, CA). Data are reported as means ± SD unless otherwise indicated. Correlations statistics were calculated according to the Spearman's rank and Pearson correlation methods.

Online supplemental material
Fig. S1 shows prove of PKN3 kinase dead inactivity, another western blot showing PKN3 phosphorylation on Thr849 influenced by p130Cas variant expression and that PKN3 colocalizes with stress fibers. Fig. S2 shows PKN3 autophosphorylation, phospho-pattern of p130Cas from suspension cells and Co-expression of human p130Cas/BCAR1 and PKN3 in prostate and breast tumors. Fig. S3 shows the influence of PKN3 and GFP-p130Cas variants expression on cell morphology and proliferation. Fig. S4 shows that PKN3 induction doesn't change activation status of STAT3, ERK, Akt, MLC and mTOR signaling (only slightly increase Src activity) in cells growing on plastic and that PKN3 dependent invasiveness is independent of phosphorylation in p130Cas SRD. Fig. S5 shows that PKN3 crosstalk with Src is p130Cas dependent. Furthermore, provides additional information relevant to tumors and metastasis. Fig. S6 shows that PKN3 binds strongly to p130Cas SH3 domain and do not bind to p130Cas SRD domain. Movies S1-S3 show that only PKN3 WT clearly localizes to lamellipodia of p130Cas-/- MEFs re-expressing p130Cas co-transfected by GFP-PKN3 variants and mCherry-LifeActin. Movie S4-5 show (3D cell zone exclusion assay) that PKN3 increases cell migration velocity in collagen only in the presence of p130Cas. Tables S1 and S2, included as an Excel files, provide a list of synthetized cDNA sequences (geneArt) or oligonucleotides, respectively, used in this study.

Acknowledgements

This work was funded by Czech Science Foundation grants 15-17419S and 15-07321S, by the Ministry of Education, Youth and Sports of CR within the LQ1604 National Sustainability Program II (Project BIOCEV-FAR), LQ1601 (Project CEITEC 2020), by the project „BIOCEV" (CZ.1.05/1.1.00/02.0109), and by Charles University Grant Agency (224217). We acknowledge the support by the MEYS CR (CZ.02.1.01/0.0/0.0/16_013/0001775 Czech-BioImaging) and the support by Imaging Methods Core Facility at BIOCEV, institution supported by the Czech-BioImaging large RI project (LM2015062 funded by MEYS CR) for their support with obtaining imaging data presented in this paper. We thank Marie Charvátová for technical help and L. Janečková for help with immunohistochemistry. We acknowledge Pfizer as the source of the Materials by providing antibody anti-phosphoThr849 of PKN3 (human Thr860).

The authors declare no competing financial interests.

Author contributions: Conceptualization, J. Gemperle, D. Rosel and J. Brábek; methodology, J. Gemperle, M. Dibus and L. Koudelková; investigation, J. Gemperle, M. Dibus, D. Rosel and J. Brábek; resources, J. Brábek; writing—original draft, J. Gemperle; writing—re-viewing, J. Gemperle, M. Dibus, D. Rosel and J. Brábek; visualization, J. Gemperle; supervision, J. Brábek and D. Rosel; funding acquisition, J. Gemperle, M. Dibus, J. Brábek and D. Rosel.

Footnotes
Abbreviations used:

BCAR1 = breast cancer anti-estrogen resistance protein 1
Dox = doxycycline
ECM = extracellular matrix
FN = fibronectin
KO = knockout
mPR = mutation P_{500}PPKPPRL to PAPSAPRL (mouse PKN3 – mutant unable to bind p130Cas)
MEFs = mouse embryonic fibroblasts
PKN3 = protein kinase N3
p130Cas = Crk-associated substrate (size 130 kDa)
RT = room temperature

RTCA = real-time cell analysis
SC = p130Cas-/- MEFs re-expressing p130Cas transformed by SrcF
SCpkn3-/- = SC PKN3 KO
SrcF = constitutively active Src (Src Y527F)
WT = wild type

References:

Aleku, M. *et al.* (2008) 'Atu027, a liposomal small interfering RNA formulation targeting protein kinase N3, inhibits cancer progression', *Cancer Res*. 2008/12/03, 68(23), pp. 9788–9798. doi: 10.1158/0008-5472.CAN-08-2428.

Astier, A. *et al.* (1997) 'The related adhesion focal tyrosine kinase differentially phosphorylates p130Cas and the Cas-like protein, p105HEF1.', *The Journal of biological chemistry*, 272(32), pp. 19719–24. doi: 10.1074/jbc.272.32.19719.

Brábek, J. *et al.* (2004) 'CAS promotes invasiveness of Src-transformed cells', *Oncogene*. 2004/07/27, 23(44), pp. 7406–7415. doi: 10.1038/sj.onc.1207965.

Brábek, J. *et al.* (2005) 'Crk-associated substrate tyrosine phosphorylation sites are critical for invasion and metastasis of Src-transformed cells', *Molecular Cancer Research*, 3(6), pp. 307–315. doi: 10.1158/1541-7786.MCR-05-0015.

Braniš, J. *et al.* (2017) 'The role of focal adhesion anchoring domains of CAS in mechanotransduction', *Scientific reports*. Nature Publishing Group, 7, p. 46233. doi: 10.1038/srep46233.

Cabodi, S. *et al.* (2004) 'p130Cas interacts with estrogen receptor alpha and modulates non-genomic estrogen signaling in breast cancer cells', *J Cell Sci*. 2004/03/17, 117(Pt 8), pp. 1603–1611. doi: 10.1242/jcs.01025.

Cabodi, S. *et al.* (2006) 'p130Cas as a New Regulator of Mammary Epithelial Cell Proliferation, Survival, and HER2-Neu Oncogene-Dependent Breast Tumorigenesis', *Cancer Research*, 66(9), pp. 4672–4680. doi: 10.1158/0008-5472.CAN-05-2909.

Cabodi, S., del Pilar Camacho-Leal, M., *et al.* (2010) 'Integrin signalling adaptors: not only figurants in the cancer story', *Nat Rev Cancer*. 2010/11/26. Nature Publishing Group, a division of Macmillan Publishers Limited. All Rights Reserved., 10(12), pp. 858–870. doi: 10.1038/nrc2967.

Cabodi, S., Tinnirello, A., *et al.* (2010) 'p130Cas is an essential transducer element in ErbB2 transformation', *FASEB J*. 2010/05/28, 24(10), pp. 3796–3808. doi: 10.1096/fj.10-157347.

Czauderna, F. *et al.* (2003) 'Inducible shRNA expression for application in a prostate cancer mouse model', *Nucleic Acids Res*. 2003/10/25, 31(21), p. e127. Available at: http://www.ncbi.nlm.nih.gov/pubmed/14576327 (Accessed: 1 June 2013).

Defilippi, P., Di Stefano, P. and Cabodi, S. (2006) 'p130Cas: a versatile scaffold in signaling networks', *Trends Cell Biol*. 2006/04/04, 16(5), pp. 257–263. doi: 10.1016/j.tcb.2006.03.003.

Donato, D. M. *et al.* (2010) 'Dynamics and mechanism of p130Cas localization to focal adhesions', *J Biol Chem*. 2010/05/01, 285(27), pp. 20769–20779. doi: 10.1074/jbc.M109.091207.

Dorssers, L. C. *et al.* (2001) 'Tamoxifen resistance in breast cancer: elucidating mechanisms.', *Drugs*, 61(12), pp. 1721–33. doi: 10.2165/00003495-200161120-00004.

Dorssers, L. C. *et al.* (2004) 'The prognostic value of BCAR1 in patients with primary breast cancer', *Clin Cancer Res*. 2004/09/28, 10(18 Pt 1), pp. 6194–6202. doi: 10.1158/1078-0432.CCR-04-0444.

Fonseca, P. M. *et al.* (2004) 'Regulation and localization of CAS substrate domain tyrosine phosphorylation', *Cell Signal*. 2004/01/31, 16(5), pp. 621–629. doi: 10.1016/j.cellsig.2003.10.004.

Fromont, G. *et al.* (2007) 'BCAR1 expression in prostate cancer: Association with 16q23 LOH status, tumor progression and EGFR/KAI1 staining', *The Prostate*, 67(3), pp. 268–273. doi: 10.1002/pros.20516.

Fromont, G. and Cussenot, O. (2011) 'The integrin signalling adaptor p130CAS is also a key player in prostate cancer', *Nat Rev Cancer*. 2011/02/25, 11(3), p. 227. doi: doi: nrc2967-c1.

Gao, J. *et al.* (2013) 'Integrative Analysis of Complex Cancer Genomics and Clinical Profiles Using the cBioPortal', *Science Signaling*, 6(269), pp. pl1-pl1. doi: 10.1126/scisignal.2004088.

Garcia-Guzman, M. *et al.* (1999) 'Cell adhesion regulates the interaction between the docking protein p130(Cas) and the 14-3-3 proteins', *J Biol Chem*. 1999/02/20, 274(9), pp. 5762–5768. doi: 10.1074/jbc.274.9.5762.

Gemperle, J. *et al.* (2017) 'Structural characterization of CAS SH3 domain selectivity and regulation reveals new CAS interaction partners', *Scientific reports*, (May), pp. 1–18. doi: 10.1038/s41598-017-08303-4.

Hashimoto, T. *et al.* (1998) 'Localization of PKN mRNA in the rat brain', *Brain Res Mol Brain Res*. 1998/09/05, 59(2), pp. 143–153. doi: 10.1016/S0169-328X(98)00155-7.

Hivert, V., Pierre, J. and Raingeaud, J. (2009) 'Phosphorylation of human enhancer of filamentation (HEF1) on serine 369 induces its proteasomal degradation', *Biochem Pharmacol*. 2009/06/23, 78(8), pp. 1017–1025. doi: 10.1016/j.bcp.2009.06.005.

Honda, H. *et al.* (1998) 'Cardiovascular anomaly, impaired actin bundling and resistance to Src-induced transformation in mice lacking p130Cas', *Nat Genet*. 1998/08/11, 19(4), pp. 361–365. doi: 10.1038/1246.

Janoštiak, R. *et al.* (2011) 'Tyrosine Phosphorylation within the SH3 domain Regulates CAS Subcellular Localization, Cell Migration, and Invasiveness', *Mol Biol Cell*. 2011/09/23, 22(22), pp. 4256–4267. doi: 10.1091/mbc.E11-03-0207.

Janoštiak, R. *et al.* (2014) 'CAS directly interacts with vinculin to control mechanosensing and focal adhesion dynamics.', *Cellular and molecular life sciences : CMLS*, 71(4), pp. 727–44. doi: 10.1007/s00018-013-1450-x.

Kang, H. *et al.* (2015) 'Downregulation of microRNA-362-3p and microRNA-329 promotes tumor progression in human breast cancer.', *Cell death and differentiation*. Nature Publishing Group, 23(3), pp. 484–495. doi: 10.1038/cdd.2015.116.

Lachmann, S. *et al.* (2011) 'Regulatory Domain Selectivity in the Cell-Type Specific PKN-Dependence of Cell Migration', *PLoS One*, 6(7). doi: e2173210.1371/journal.pone.0021732.

Leenders, F. *et al.* (2004) 'PKN3 is required for malignant prostate cell growth downstream of activated PI 3-kinase', *EMBO J*. 2004/07/30, 23(16), pp. 3303–3313. doi: 10.1038/sj.emboj.7600345 7600345.

Lim, W. G. *et al.* (2008) 'The C-terminus of PRK2/PKNgamma is required for optimal activation by RhoA in a GTP-dependent manner.', *Archives of biochemistry and biophysics*, 479(2), pp. 170–8. doi: 10.1016/j.abb.2008.09.008.

Makkinje, A. *et al.* (2009) 'AND-34/BCAR3 regulates adhesion-dependent p130Cas serine phosphorylation and breast cancer cell growth pattern', *Cell Signal*. 2009/05/21, 21(9), pp. 1423–1435. doi: 10.1016/j.cellsig.2009.05.006.

Mellor, H. *et al.* (1998) ‘PRK1 is targeted to endosomes by the small GTPase, RhoB’, *J Biol Chem*. 1998/03/28. American Society for Biochemistry and Molecular Biology, 273(9), pp. 4811–4814. doi: 10.1074/JBC.273.9.4811.

Mukai, H. *et al.* (2016) ‘PKN3 is the major regulator of angiogenesis and tumor metastasis in mice.’, *Scientific reports*, 6, p. 18979. doi: 10.1038/srep18979.

Mukai, H. and Ono, Y. (1994) ‘A Novel Protein Kinase with Leucine Zipper-like Sequences: Its Catalytic Domain Is Highly Homologous to That of Protein Kinase C’, *Biochemical and Biophysical Research Communications*, 199(2), pp. 897–904. doi: 10.1006/bbrc.1994.1313.

Nagai, Y. *et al.* (2013) ‘p130Cas, Crk-associated substrate, plays important roles in osteoclastic bone resorption.’, *Journal of bone and mineral research : the official journal of the American Society for Bone and Mineral Research*, 28(12), pp. 2449–62. doi: 10.1002/jbmr.1936.

Nick, A. M. *et al.* (2011) ‘Silencing of p130cas in ovarian carcinoma: a novel mechanism for tumor cell death.’, *Journal of the National Cancer Institute*. 2011/10/01, 103(21), pp. 1596–612. doi: 10.1093/jnci/djr372.

Nikonova, A. S. *et al.* (2014) ‘CAS proteins in health and disease: An update’, *IUBMB Life*, 66(6), pp. 387–395. doi: 10.1002/iub.1282.

Oishi, K. *et al.* (1999) ‘Identification and characterization of PKNbeta, a novel isoform of protein kinase PKN: expression and arachidonic acid dependency are different from those of PKNalpha’, *Biochem Biophys Res Commun*. 1999/08/12, 261(3), pp. 808–814. doi: 10.1006/bbrc.1999.1116.

Piccinini, F., Kiss, A. and Horvath, P. (2015) ‘CellTracker (not only) for dummies.’, *Bioinformatics (Oxford, England)*, p. btv686-. doi: 10.1093/bioinformatics/btv686.

Pylayeva, Y. *et al.* (2009) ‘Ras- and PI3K-dependent breast tumorigenesis in mice and humans requires focal adhesion kinase signaling’, *J Clin Invest*. 2009/01/17, 119(2), pp. 252–266. doi: 10.1172/JCI37160.

Quilliam, L. A. *et al.* (1996) ‘Isolation of a NCK-associated kinase, PRK2, an SH3-binding protein and potential effector of Rho protein signaling’, *J Biol Chem*. 1996/11/15, 271(46), pp. 28772–28776. doi: 10.1074/jbc.271.46.28772.

Ran, F. A. *et al.* (2013) ‘Genome engineering using the CRISPR-Cas9 system.’, *Nature protocols*, 8(11), pp. 2281–308. doi: 10.1038/nprot.2013.143.

Riedl, J. *et al.* (2008) ‘Lifeact: a versatile marker to visualize F-actin’, *Nature Methods*, 5(7), pp. 605–607. doi: 10.1038/nmeth.1220.

Ruest, P. J. *et al.* (2001) ‘Mechanisms of CAS substrate domain tyrosine phosphorylation by FAK and Src’, *Mol Cell Biol*. 2001/10/18, 21(22), pp. 7641–7652. doi: 10.1128/MCB.21.22.7641-7652.2001.

Santel, A. *et al.* (2010) ‘Atu027 prevents pulmonary metastasis in experimental and spontaneous mouse metastasis models.’, *Clinical cancer research : an official journal of the American Association for Cancer Research*, 16(22), pp. 5469–80. doi: 10.1158/1078-0432.CCR-10-1994.

Schindelin, J. *et al.* (2012) ‘Fiji: an open-source platform for biological-image analysis’, *Nature Methods*. Nature Publishing Group, 9(7), pp. 676–682. doi: 10.1038/nmeth.2019.

Schultheis, B. *et al.* (2014) ‘First-in-human phase I study of the liposomal RNA interference therapeutic Atu027 in patients with advanced solid tumors.’, *Journal of clinical oncology : official journal of the American Society of Clinical Oncology*, 32(36), pp. 4141–8. doi: 10.1200/JCO.2013.55.0376.

Strumberg, D. *et al.* (2012) ‘Phase I clinical development of Atu027, a siRNA formulation targeting PKN3 in patients with advanced solid tumors’, *Int J Clin Pharmacol Ther*. 2011/12/24, 50(1), pp. 76–78. doi: 10.5414/CPP50076.

Ta, H. Q. *et al.* (2008) ‘A Novel Association between p130Cas and Resistance to the Chemotherapeutic Drug Adriamycin in Human Breast Cancer Cells’, *Cancer Research*, 68(21), pp. 8796–8804. doi: 10.1158/0008-5472.CAN-08-2426.

Tarone, G. *et al.* (1985) ‘Rous sarcoma virus-transformed fibroblasts adhere primarily at discrete protrusions of the ventral membrane called podosomes.’, *Experimental cell research*, 159(1), pp. 141–57. doi: 10.1016/S0014-4827(85)80044-6.

Tazaki, T. *et al.* (2008) ‘Functional analysis of Src homology 3-encoding exon (exon 2) of p130Cas in primary fibroblasts derived from exon 2-specific knockout mice’, *Genes Cells*. 2008/02/01, 13(2), pp. 145–157. doi: 10.1111/j.1365-2443.2007.01156.x.

Tikhmyanova, N., Little, J. L. and Golemis, E. A. (2010) ‘CAS proteins in normal and pathological cell growth control’, *Cellular and Molecular Life Sciences*, 67(7), pp. 1025–1048. doi: 10.1007/s00018-009-0213-1.

Tornillo, G., Defilippi, P. and Cabodi, S. (2014) ‘Cas proteins: dodgy scaffolding in breast cancer’, *Breast Cancer Research*, 16(5), p. 443. doi: 10.1186/s13058-014-0443-5.

Van Troys, M. *et al.* (2018) ‘Analysis of Invasion Dynamics of Matrix-Embedded Cells in a Multisample Format’, in *Methods in molecular biology (Clifton, N.J.)*, pp. 79–117. doi: 10.1007/978-1-4939-7701-7_9.

Uehara, S. *et al.* (2017) ‘Protein kinase N3 promotes bone resorption by osteoclasts in response to Wnt5a-Ror2 signaling.’, *Science signaling*, 10(494). doi: 10.1126/scisignal.aan0023.

Unsal-Kacmaz, K. *et al.* (2011) ‘The interaction of PKN3 with RhoC promotes malignant growth’, *Mol Oncol*. 2012/01/06. doi: 10.1016/j.molonc.2011.12.001.

Vincent, S. and Settleman, J. (1997) ‘The PRK2 kinase is a potential effector target of both Rho and Rac GTPases and regulates actin cytoskeletal organization’, *Mol Cell Biol*. 1997/04/01, 17(4), pp. 2247–2256. doi: 10.1128/MCB.17.4.2247.

Figures

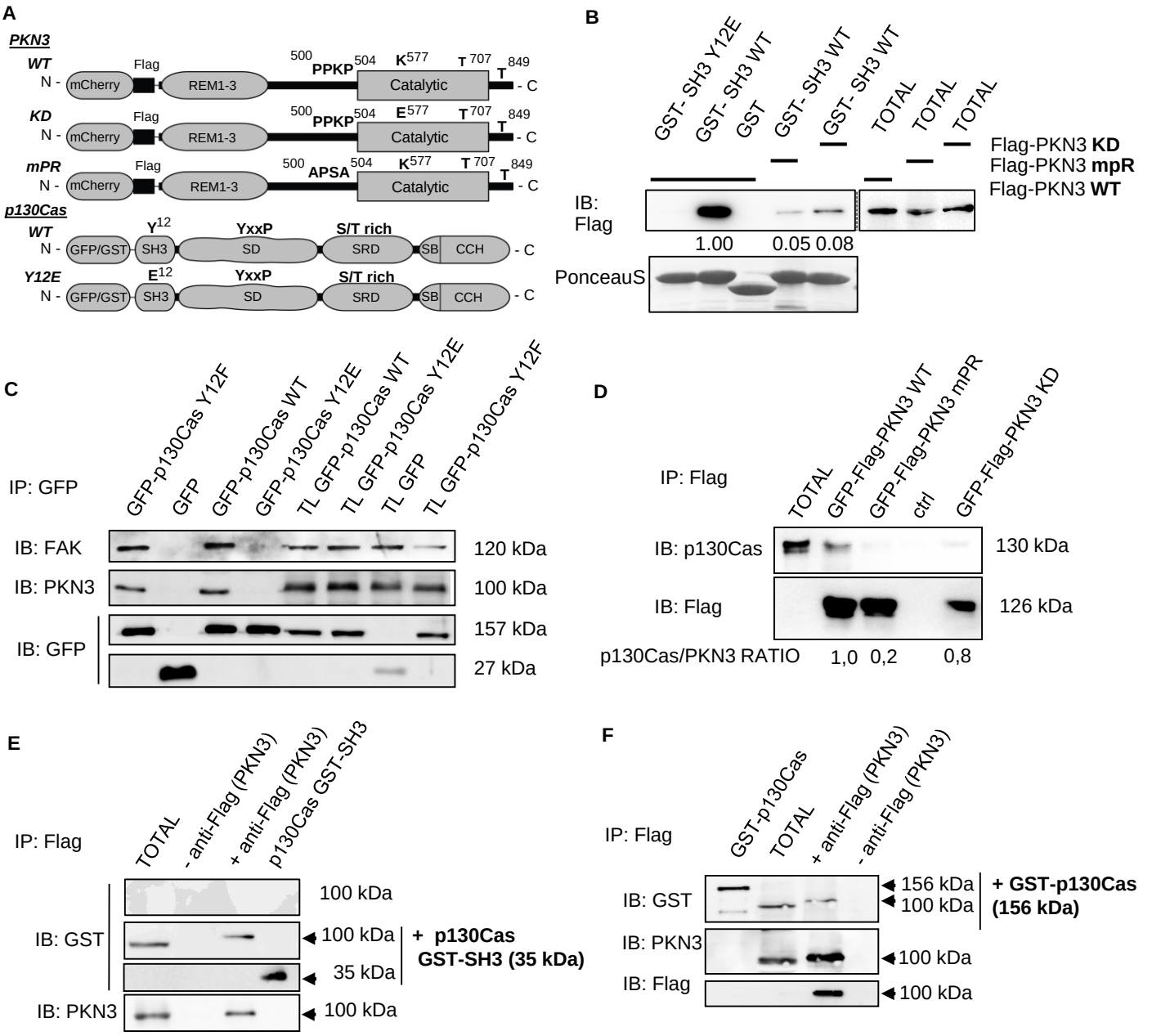

Figure 1. p130Cas directly interacts with PKN3 **A)** Schematic representation of PKN3 and p130Cas domains, important residues and their mutagenesis. **B)** Purified GST fused p130Cas SH3 variants (WT, Y12E) were used to pull-down Flag-PKN3 variants (WT, mPR, KD), expressed in MEFs. Pulled-down proteins were immunoblotted with anti-Flag antibody, and GST-SH3 domains were stained with Ponceau-S. GST with lysate from Flag-PKN3 WT was used as a negative control. **C-D)** Binding of PKN3 to full-length p130Cas was verified by co-immunoprecipitations. **C**) The MDA-MB-231 cells were transiently transfected with indicated mouse GFP-p130Cas variants or GFP alone followed by immunoprecipitations using anti-GFP antibody. Co-immunoprecipitated PKN3 and FAK (as a positive control) were detected using anti-PKN3 antibody or anti-FAK, respectively. **D**) The MDA-MB-231 cells were transiently transfected with mouse Flag and GFP-fused PKN3 variants (WT, mPR, KD) followed by immunoprecipitations using anti-Flag sepharose and co-immunoprecipitated p130Cas was detected by anti-p130Cas antibody. In far western experiments **E-F**) Flag-PKN3 was immunoprecipitated from transfected MDA-MB-231 cells, transferred to nitrocellulose membrane and incubated with **E)** recombinant GST-p130Cas SH3 domain or **F)** whole GST-p130Cas followed by detection with anti-GST antibody. The membrane was then stripped and both endogenous (endo PKN3) as well as exogenous PKN3 (exo Flag-PKN3) were detected by anti-PKN3 and anti-Flag antibody, respectively. The upper membrane in fig. E was not incubated with recombinant GST-p130Cas SH3 domain and represents a negative control for anti GST antibody. As a positive control for GST cross-reactivity a purified GST-p13Cas SH3 in **E)** or whole GST-p130Cas in **F)** was ran alongside.

TL or TOTAL: total cell lysate; IP: immunoprecipitation; Ctrl: control samples prepared from untransfected MDA-MB-231 cells.

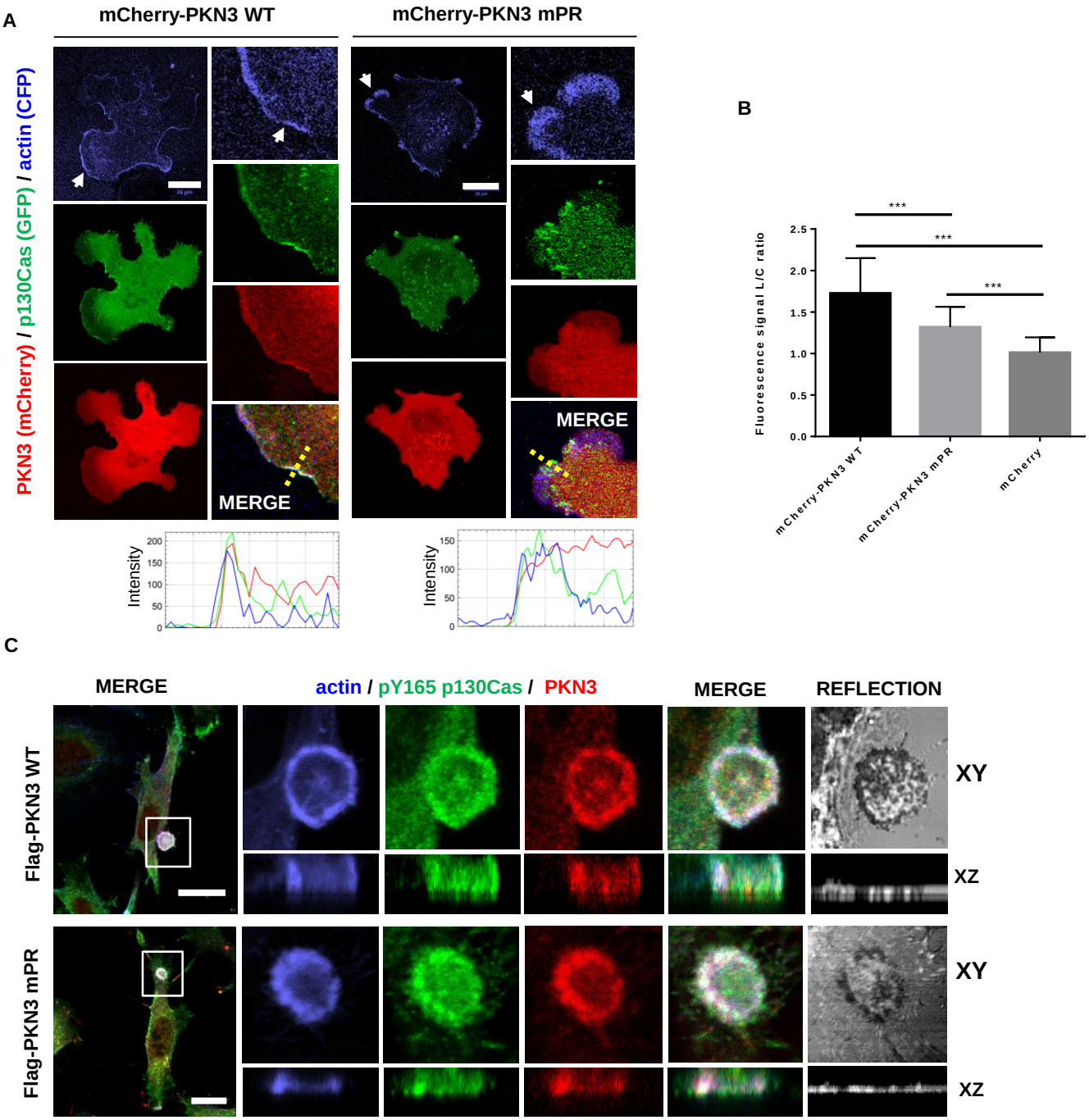

Figure 2. PKN3 colocalizes with p130Cas in lamellipodia and podosome rosettes. Representative images are shown. **A)** p130Cas-/- MEFs plated on fibronectin (FN) were transfected by GFP-p130Cas, CFP-LifeAct and mCherry-PKN3WT or mCherry-PKN3 mPR and imaged live 24 hours after transfection. White arrow indicates lamellipodia. Histogram of dotted straight line is shown. **B)** Quantification of mCherry-PKN3 WT, mCherry-PKN3 mPR and mCherry localization to lamellipodia (LifeAct as marker) was calculated as described in methods (values are mean ± standard deviation (SD) from three independent experiments, n>50 measurements – 3 per cell; *P<0,001, one-way ANOVA on ranks followed by Dunn´s post-hoc test). **C)** SrcF transformed p130Cas-/- MEFs co-expressing p130Cas (SC) and mouse Flag tagged PKN3 WT or Flag-PKN3 mPR are shown. Cells were grown on FN-coated coverslips for 48 hours, fixed and stained for p130Cas by anti-p165Y p130Cas antibody (2nd 405), for actin by Phalloidin 488 and for Flag-PKN3 by anti-Flag antibody (2nd 633). Reflection (670 nm) indicates fibronectin degradation. All scale bars represent 20 µm. Cell were imaged by Leica TCS SP8 microscope system equipped with Leica 63×/1.45 oil objective**.**

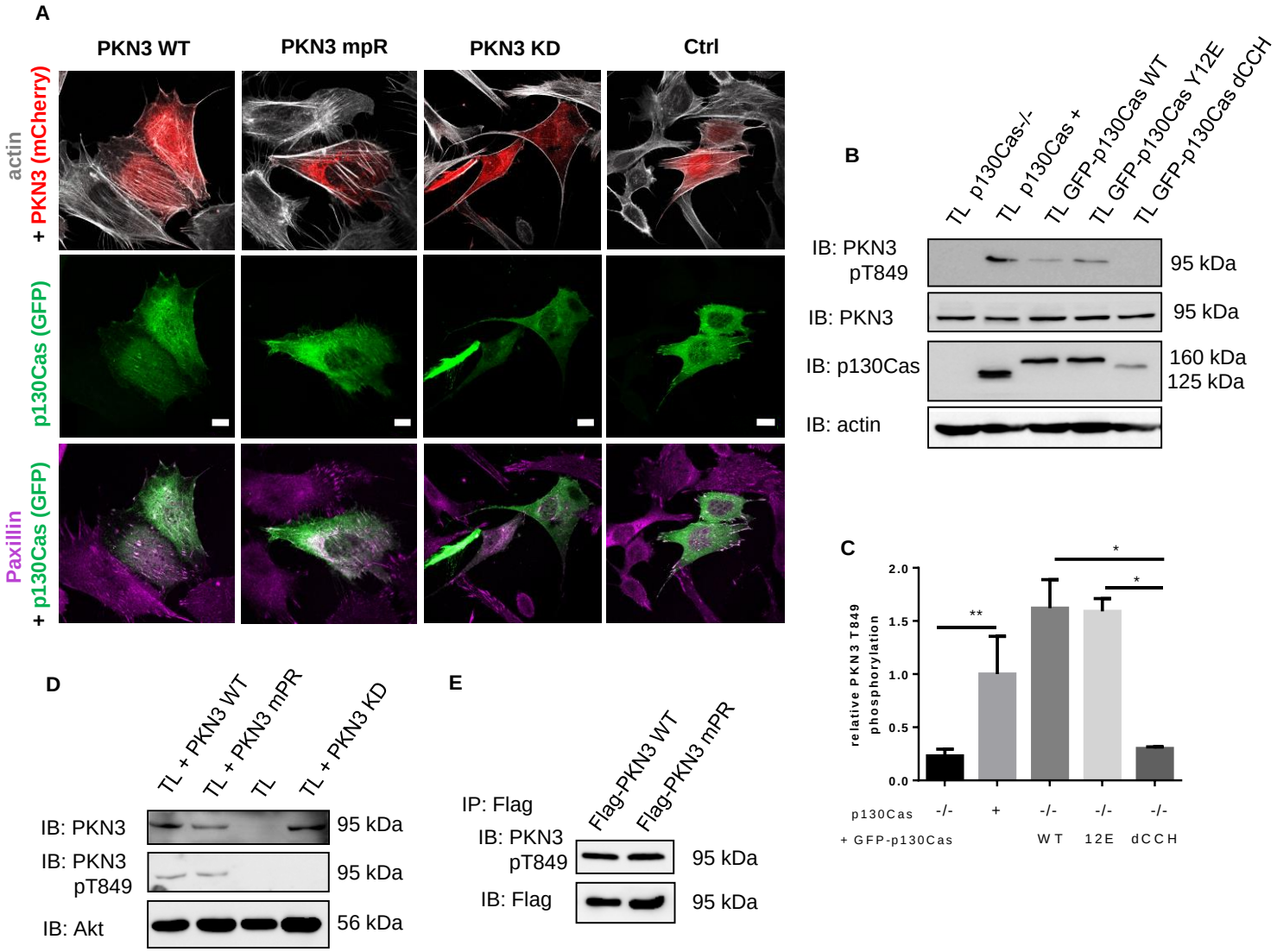

Figure 3. PKN3 activity is important for stress fibers formation and is stimulated by expression of p130Cas. **A)** p130Cas-/- MEFs cells growing on FN-coated cover slips were co-transfected by GFP-p130Cas and mCherry-PKN3 fusion variant (WT, mPR, KD) or mCherry. After 48 hours cells were fixed and imaged by Leica TCS SP2 microscope (63×/1.45 oil objective). Stress fibers were visualized by Phalloidin (405) and focal adhesions by anti-Paxillin staining (2nd 633). Representative images are shown. Scale bars represent 20 µm. **B)** p130Cas-/- MEFs or p130Cas-/- MEFs re-expressing p130Cas or transfected by GFP fused p130Cas variants (WT, YE, dCCH) were lysed in RIPA buffer, blotted to nitrocellulose membrane and analyzed for endogenous PKN3 activity by antibody anti-phosphoThr849 of PKN3 (pT849 PKN3). Expression of p130Cas mutants was verified by anti-p130Cas antibody and loading by anti-PKN3 and anti-actin antibody. **C)** Densitometric quantification of PKN3 activity (pT849 PKN3 phosphorylation). Error bars indicate means ± SD from three independent experiments. Statistical significance was evaluated by one-way repeated ANOVA followed by Turkey´s post-hoc test. **D)** Lysates or **E)** immunoprecipitates (by Flag-sepharose) from p130Cas-/- MEFs re-expressing p130Cas and overexpressing PKN3 variants (WT, mPR, KD) were immunoblotted by anti-PKN3, anti-pT849 PKN3 and anti-Akt antibodies (loading control).

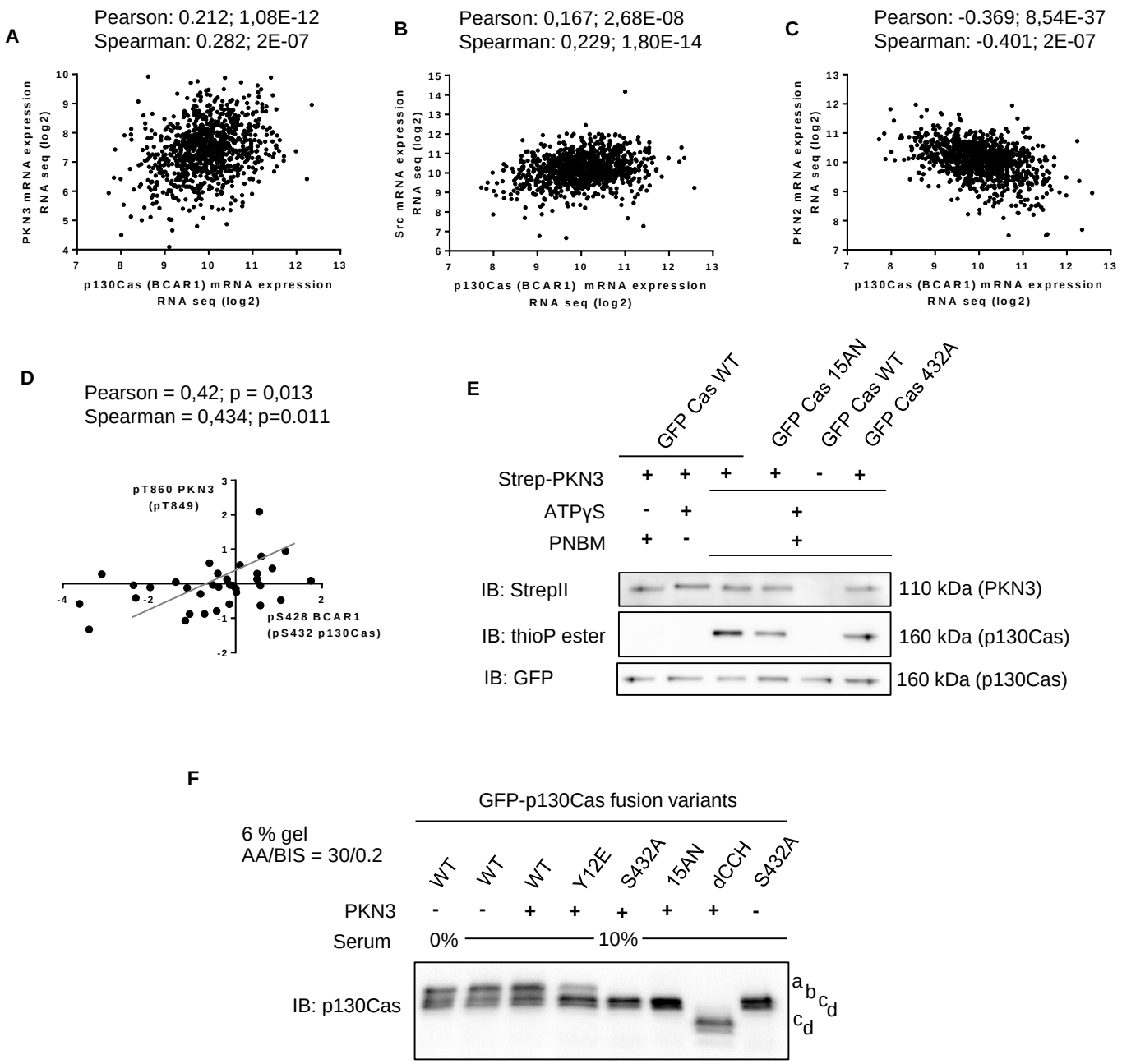

Figure 4. PKN3 phosphorylates p130Cas and PKN3 activity correlates with p130Cas phosphorylation in human breast carcinomas. **A-C)** Correlation statistics (graphs) of publicly available RNA seq data of co-expression of **A)** human p130Cas/BCAR1 and PKN3; **B)** p130Cas/BCAR1 and Src; **C)** p130Cas/BCAR1 and PKN2 or graph **D)** showing positive linear dependency of protein phosphorylation levels (log ratio values) of PKN3 Thr860 and p130Cas/BCAR1 Ser428 in invasive human breast tumors. **E)** Kinase reactions in vitro with precipitated Strep-PKN3 and GFP fusion p130Cas variants (shown as Cas). Reactions were carried out in the presence of ATPγS followed by alkylation with PNBM and detection with specific anti-thiophosphate esters (thioP ester) antibody. Combinations of PNBM (alkylation reagent) or ATPγS were facilitated to exclude false positive signals. Antibodies anti-StrepII and GFP were used to detect PKN3 kinase or GFP fused p130Cas variants, respectively. Representative blots are shown. **F)** Lysates from p130Cas-/- MEFs re-expressing GFP fused p130Cas variants with or without mCherry-PKN3 overexpression were run on SDS-PAGE using an acrylamide/bisacrylamide ratio of 30:0.2 followed by immunoblotting and detection by anti-p130Cas antibody. a-d refers to different GFP-p130Cas isoforms.

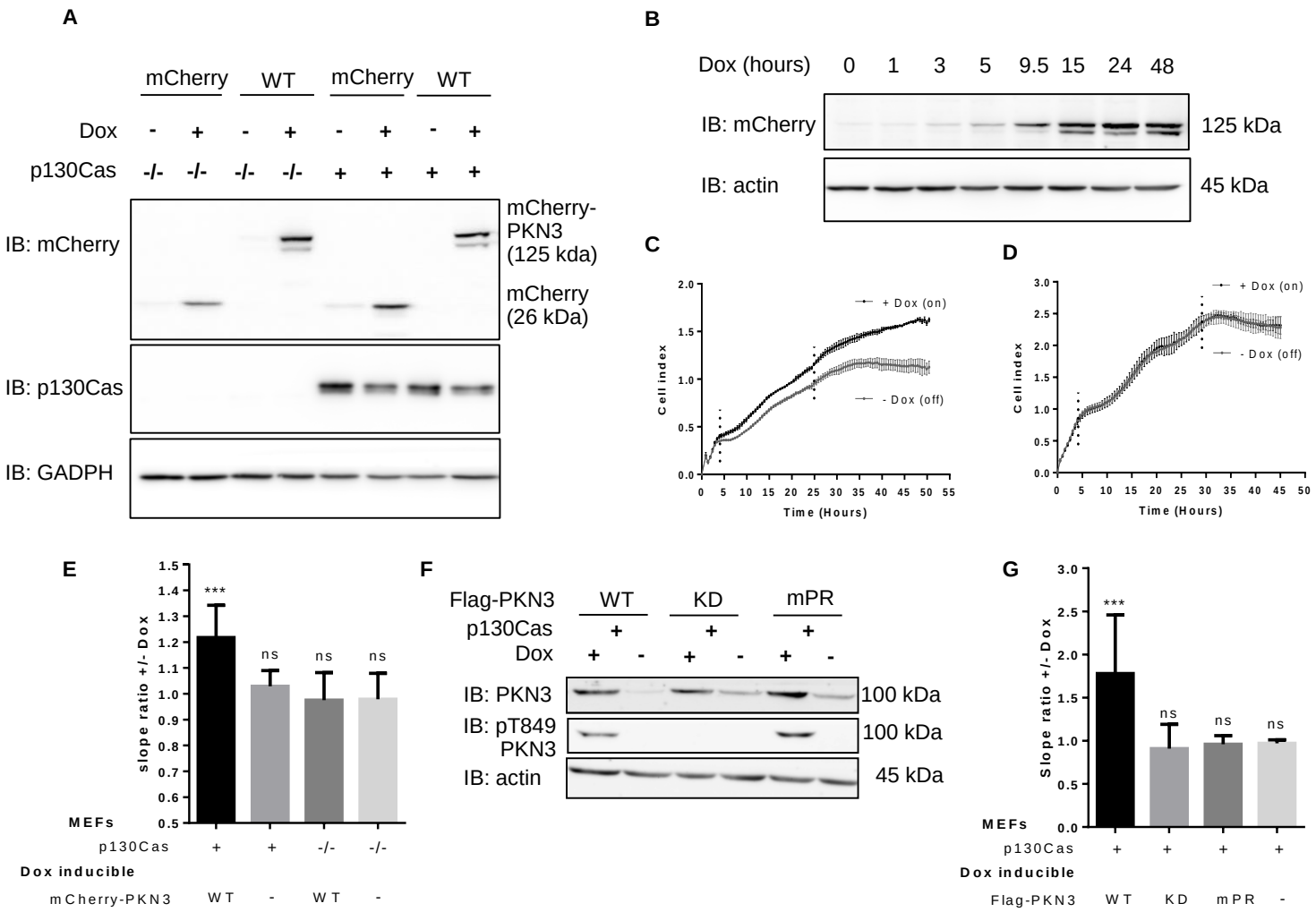

Figure 5. PKN3 overexpression regulates growth of MEFs and this effect requires PKN3 – p130Cas interaction. **A)** Immunoblotted lysates from MEFs p130Cas-/- or MEFs p130Cas-/- re-expressing p130Cas (p130Cas+) treated by doxycycline to induce expression of mCherry-PKN3 or mCherry alone. p130Cas presence was detected by ani-p130Cas antibody and mCherry epitope by anti-mCherry antibody. **B)** Dynamics of mCherry-PKN3 expression after supplementation with doxycycline shown by immunoblot with anti-mCherry antibody. **C-E)** Effect of induced mCherry-PKN3 expression on cell growth. Representative graphs showing growth of MEFs p130Cas/ re-expressing p130Cas (p130Cas+) **C)** or MEFs p130Cas/ **D)** measured in real-time using the xCELLigance RTCA (real-time cell analysis) system instrument. **E)** Quantification of cell growth change induced by mCherry-PKN3 expression ("-" indicates inducible mCherry expression used as negative control). Slope ratios reflecting cell growth were calculated from the log growth phase of cell growth (indicated by dotted lines (see C), D)). **F)** Immunoblotted lysates from MEFs p130Cas-/- re-expressing p130Cas (p130Cas+) treated or not treated by doxycycline which induced expression of Flag fused PKN3 variants (WT, mPR, KD, empty vector). Stimulated overexpression of PKN3 was detected by anti-PKN3 antibody and its activity by antibody anti-pT849 PKN3. **G)** Quantification of cell growth change stimulated by Dox-inducible expression of Flag fused PKN3 variants (WT, mPR, KD) in MEFs p130Cas-/- re-expressing p130Cas (p130Cas+).

All error bars indicate means ± SD calculated from 3-5 independent experiments (each in triplicates). Statistical significance was always calculated between induced and non-induced cells and evaluated by one-way repeated ANOVA followed by Turkey post-hoc test (***P < 0.001).

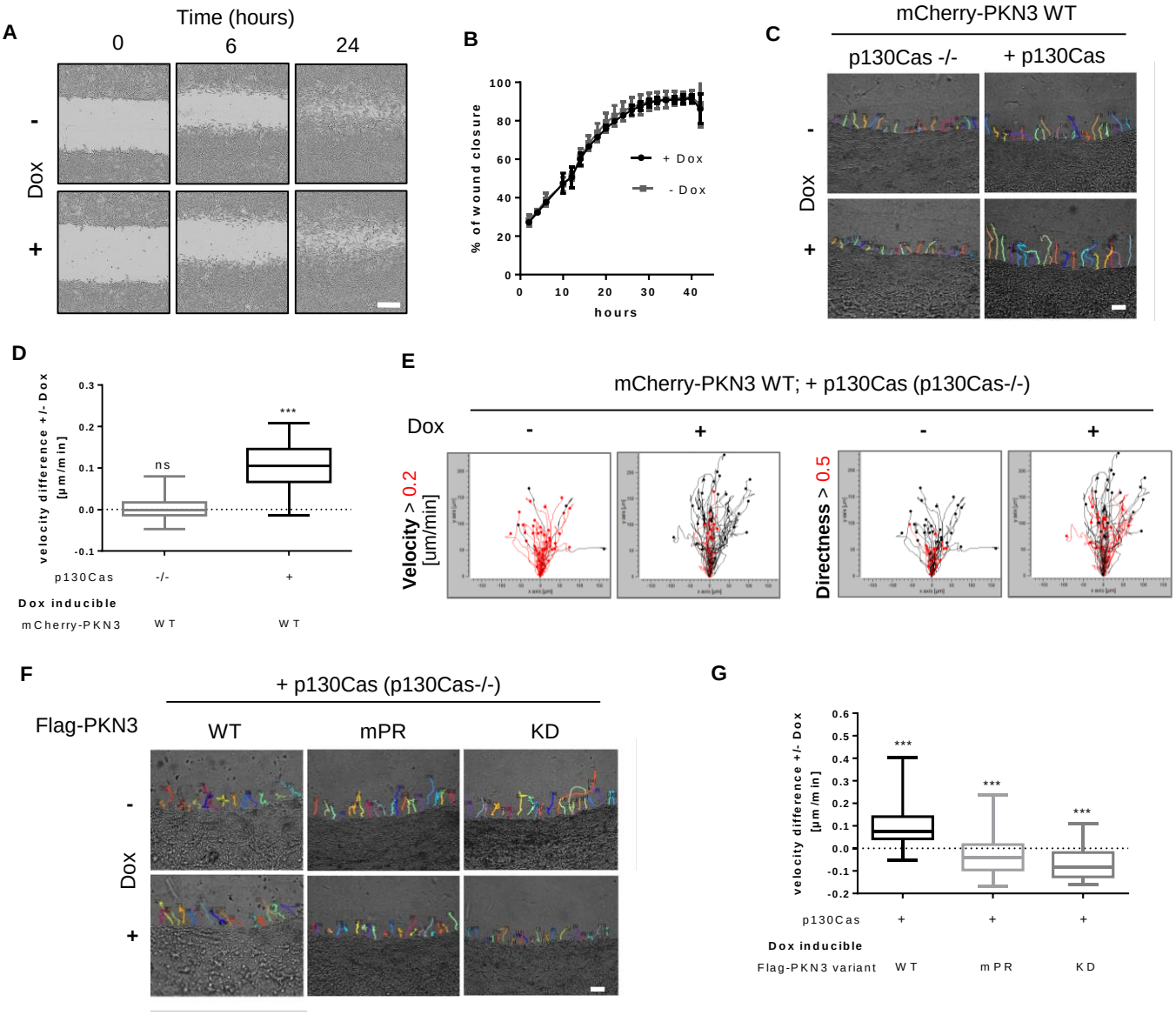

Figure 6. The interaction of p130Cas with PKN3 is required for PKN3-dependent increase of invasiveness but not 2D migration. **A)** 2D migration analyzed by wound healing assay. Representative images of MEFs p130Cas-/- re-expressing p130Cas with or without 24 hours pre-induced for Flag-PKN3 expression at the time of wounding (0 h), after 6 and 24 hours are shown (scale bar 300 µm). **B)** Representative graph of wound closure of cells shown in A). **C-G)** Cell invasiveness analyzed by 3D cell-zone exclusion assay. Cell migration into collagen was recorded using time-lapse video microscopy with frames being collected every 5 min for 18 hours, starting 2 hours after collagen scratch, with or without Dox supplementation. Expression of different constructs was pre-induced day before. **C)** Representative tracking maps of cells (MEFs p130Cas-/- or MEFs p130Cas-/- re-expressing p130Cas) migrating into collagen supplemented with or without doxycycline for induction of mCherry-PKN3 expression (scale bar 100 µm). Relevant supplemental movies S4-5 are included. **D)** Quantification of cell migration velocity difference induced by doxycycline inducible mCherry-PKN3 expression in the p130Cas null background with or without re-expression of p130Cas. **E)** Migration maps comparing the velocity and directionality of cells described in D). The boxed traces represent the length (above 0.2 µm black, below red) and directionality (above 0.5 black, below red) of cell movement of each individually tracked cell plotted from the same point of origin. **F)** Representative tracking maps of MEFs p130Cas-/- re-expressing p130Cas migrating into collagen supplemented with or without doxycycline for induction of Flag-PKN3 variant expression as indicated (scale bar 100 µm) and their quantification **G)**.
Box and whisker graphs show quantification of cell migration into collagen out of 3 independent experiments (n=60 cells). Statistical significance comparing induced and non-induced cells was evaluated by one-way ANOVA or one-way ANOVA on ranks followed by Turkey post-hoc test (***P < 0.001).

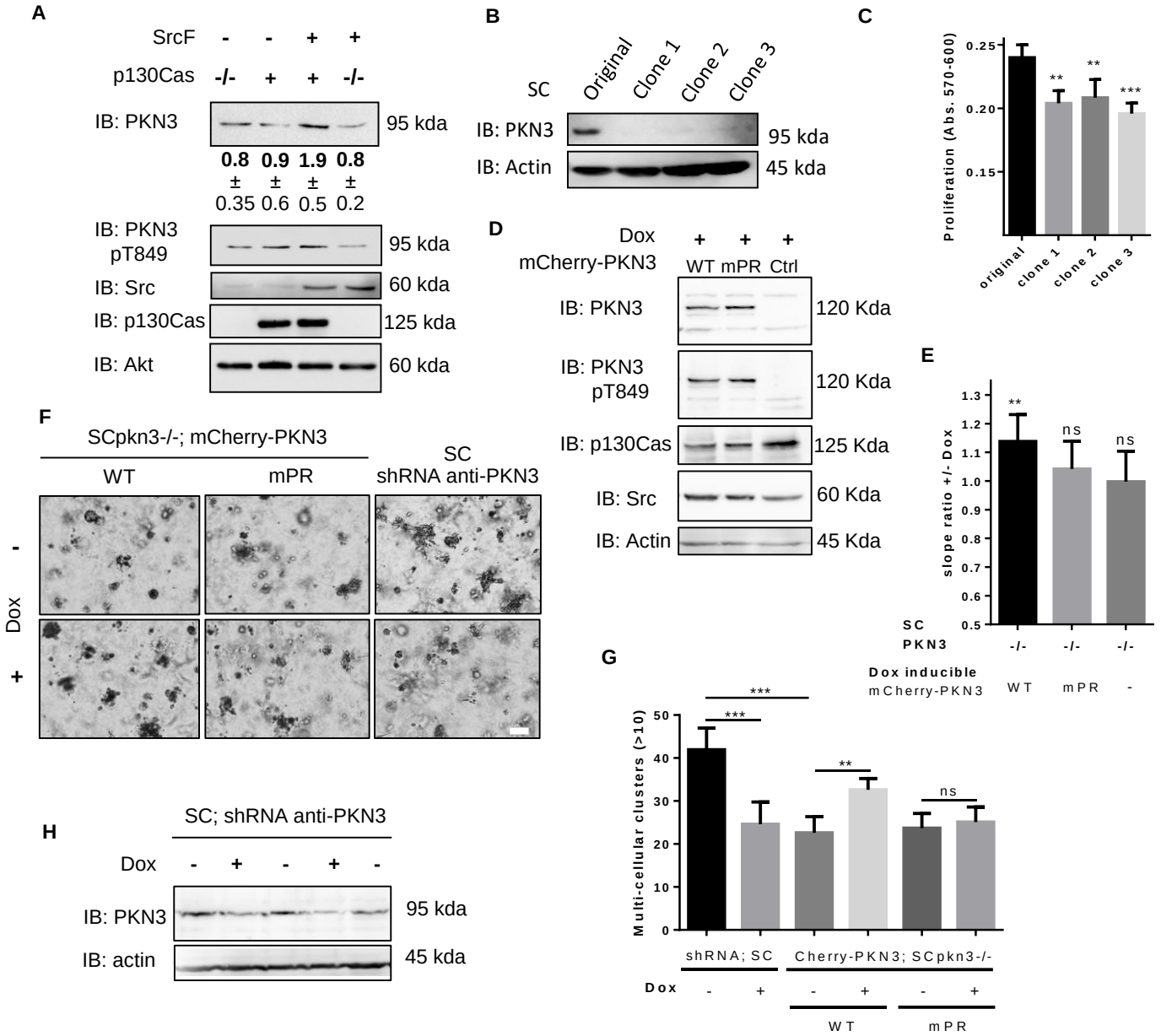

Figure 7. PKN3 regulates growth in 2D and in 3D environment of SrcF-transformed MEFs through interaction with p130Cas. **A)** Immunoblotted lysates from MEFs p130Cas-/- re-expressing p130Cas with or without transformation by constitutively active Src (SrcF, SC cells). Src and p130Cas were detected by corresponding antibodies anti-Src or anti-p130Cas, respectively. Antibodies anti-PKN3 or anti-pT849 PKN3 were used for PKN3 and anti-Akt served as loading control. Densitometric quantification of protein PKN3 amount is indicated below. **B)** Immunoblot of SC cells and SC cells with PKN3 gene inactivation by CRISPR/CAS9 (SCpkn3-/-). Inactivation of PKN3 expression is visualized by antibody anti-PKN3. Antibody anti-actin was used as loading control. **C)** Quantification of SC cells proliferation rate with or without inactivated PKN3 gene cassette by AlamarBlue method (72 hours after cell seeding). The graph shows mean absorbance measurement at 570 nm with reference at 600 nm corrected for the initial deviations of cell seeding counts. **D)** Immunoblotted lysates from SCpkn3-/- cells treated by doxycycline to induce expression of mCherry-PKN3, mCherry-PKN3 mPR or mCherry alone. PKN3 constructs were detected by anti-PKN3 and anti-pT849 PKN3antibodies. Src and p130Cas were detected by anti-Src or anti-p13Cas antibodies, respectively. Antibody anti-actin served as loading control. **E)** Quantification of cell growth change induced by Dox-inducible mCherry, mCherry-PKN3 WT or mCherry-PKN3 mPR expression in SCpkn3-/- cells measured by xCELLigence RTCA system. Slope ratios reflecting cell growth were calculated from the log growth phase of cell growth (representative curves are shown in supplementary figure S5B). **F)** SC and SCpkn3-/- cells stably expressing mCherry-PKN3 WT, mPR or shRNA anti-PKN3 in Dox-dependent manner were embedded into Matrigel. Photographs were taken on day 7, scale bar represents 100 µm; enlarged image for each sample is shown with subtracted background by ImageJ. **G)** Multi-cellular clusters (>10 cells) indicating proliferating cells were quantified relative to individual cells or small cell aggregates on day 7. Average mean is shown. **H)** Immunoblot analysis showing effectiveness of PKN3 knockdown in SC cells. Antibody anti-actin was used as loading control.

All error bars indicate means ± SD calculated from 3-5 independent experiments (each in triplicates C), E); in duplicates G)). Statistical significance comparing induced and non-induced cells (E, G) was evaluated by one-way repeated ANOVA followed by Turkey post-hoc test (**P < 0.01), among variants/groups (C, G) by one-way ANOVA followed by Turkey post-hoc test (**P < 0.01; ***P < 0.001).

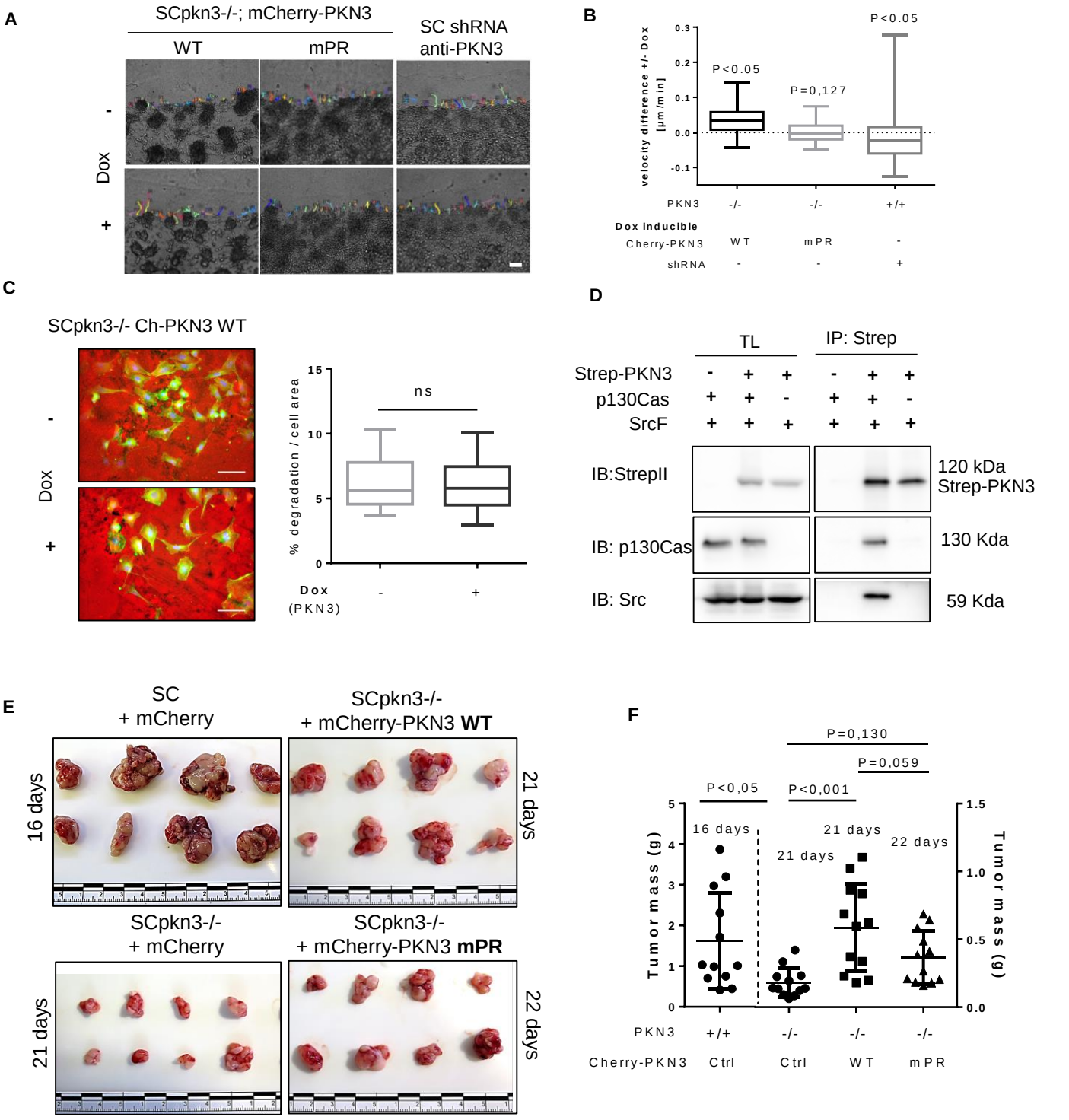

Figure 8. PKN3 regulates cell migration in 3D environment of SrcF-transformed MEFs and tumor growth in vivo through interaction with p130Cas. **A)** Representative tracking maps of SC or SCpkn3-/- cells stably expressing mCherry-PKN3 WT, mPR or shRNA anti-PKN3 in Dox-dependent manner as indicated are shown (scale bar 100 µm). Cells migrated into collagen with or without doxycycline supplementation. **B)** Quantification of cell velocity difference between induced and non-induced controls. Statistical significance was evaluated from 3-5 independent experiments by one-way ANOVA on ranks followed by Turkey post-hoc test. **C)** Gelatin degradation (Cy3-labeled) of SCpkn3-/- cells expressing dox-inducible mCherry-PKN3. Representative images are shown (On the left). Scale bar represents 100 µm. Quantification calculated as % degraded area related to total cell area stained by phalloidin 488 (on the right). **D)** Association of PKN3 with Src in p130Cas-dependent manner is shown by co-immunoprecipitations. SrcF transformed cells with or without p130Cas were transfected by Strep-PKN3 and PKN3 was precipitated by Strep-Tactin® Superflow® resin followed by western blotting and detection by anti-StrepII antibody. Coimmunoprecipitated p130Cas and Src were detected using appropriate antibodies (anti-p130Cas, anti-Src). **E)** 8 representative tumors of SC or SCpkn3-/- cells with Dox-induced mCherry, mCherry-PKN3 or mCherry-PKN3 mPR are shown with the same scale. **F)** Their respective quantification expressed as tumor mass weight at defined timescale as indicated. Statistics were evaluated by ANOVA on Ranks Dunn's Method.

TL: total cell lysate; IP: immunoprecipitation; Ctrl: control sample prepared from SC cells.